

MARTIN MARIETTA ENERGY SYSTEMS LIBRARIES



3 4456 0055479 0

ORNL/TM-9722

# ornl

**OAK RIDGE  
NATIONAL  
LABORATORY**

**MARTIN MARIETTA**

## **A Simple Procedure for Establishing Ignition Conditions in Tokamaks**

N. A. Uckan  
J. Sheffield

OAK RIDGE NATIONAL LABORATORY

CENTRAL RESEARCH LIBRARY

CIRCULATION SECTION

4500N ROOM 111

**LIBRARY LOAN COPY**

DO NOT TRANSFER TO ANOTHER PERSON

If you wish someone else to see this report, send in name with report and the library will arrange a loan.

OPERATED BY  
MARTIN MARIETTA ENERGY SYSTEMS, INC.  
FOR THE UNITED STATES  
DEPARTMENT OF ENERGY

Printed in the United States of America. Available from  
National Technical Information Service  
U.S. Department of Commerce  
5285 Port Royal Road, Springfield, Virginia 22161  
NTIS price codes—Printed Copy: A03; Microfiche A01

This report was prepared as an account of work sponsored by an agency of the United States Government. Neither the United States Government nor any agency thereof, nor any of their employees, makes any warranty, express or implied, or assumes any legal liability or responsibility for the accuracy, completeness, or usefulness of any information, apparatus, product, or process disclosed, or represents that its use would not infringe privately owned rights. Reference herein to any specific commercial product, process, or service by trade name, trademark, manufacturer, or otherwise, does not necessarily constitute or imply its endorsement, recommendation, or favoring by the United States Government or any agency thereof. The views and opinions of authors expressed herein do not necessarily state or reflect those of the United States Government or any agency thereof.

Fusion Energy Division

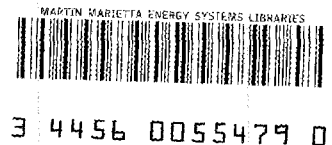
**A SIMPLE PROCEDURE FOR ESTABLISHING IGNITION  
CONDITIONS IN TOKAMAKS\***

N. A. Uckan  
J. Sheffield

\*Preprint of an invited paper presented at the Erice School on *Tokamak Startup—Problems and Scenarios Related to the Transient Phases of Ignited Tokamak Operation*, Erice, Sicily, July 14–20, 1985; proceedings to be published by Plenum Press.

Date Published—September 1985

Prepared by the  
OAK RIDGE NATIONAL LABORATORY  
Oak Ridge, Tennessee 37831  
operated by  
MARTIN MARIETTA ENERGY SYSTEMS, INC.  
for the  
U.S. DEPARTMENT OF ENERGY  
under Contract No. DE-AC05-80R21400





## CONTENTS

ABSTRACT .....	v
1 INTRODUCTION .....	1
2 GLOBAL POWER BALANCE .....	2
3 PHYSICS MODELS AND CONSTRAINTS .....	10
3.1 Plasma Current .....	10
3.2 Density Limit .....	11
3.3 Beta Limit .....	11
3.4 Confinement Models .....	13
4 CONTOUR ANALYSIS OF IGNITION CONDITIONS AND PLASMA OPERATING REGIMES .....	15
4.1 Ignition Contours .....	16
4.1.1 Neo-Alcator-like global confinement scaling .....	16
4.1.2 Combined neoclassical ion and neo-Alcator electron scalings .....	19
4.2 Heating and Operating Windows .....	21
4.3 Ignition Margin .....	23
4.4 Auxiliary Power Requirements .....	24
5 APPLICATIONS TO COMPACT TOKAMAK IGNITION EXPERIMENTS .....	25
5.1 Plasma Performance Contours for Devices with $aB_0^2/q_* \approx 20$ .....	28
5.2 Plasma Performance Contours for Devices with $(aB_0^2/q_*) \approx 32$ .....	28
6 CONCLUSION .....	28
REFERENCES .....	33



## ABSTRACT

A method of establishing ignition conditions and plasma operating regimes over large regions of parameter space ( $R_0/a$ ,  $b/a$ ,  $aB_0^2/q$ , etc.) under various physics assumptions ( $\chi_e$ ,  $\chi_i$ ,  $q_\psi$ ,  $\beta_{\text{crit}}$ ,  $n_{\text{crit}}$ , etc.) using a simple global model is presented. Contour plots of ignition, supplementary power, and plasma heating and operating windows are generated. These are then used to analyze the potential physics design space, operating regimes, and plasma performance characteristics of small ( $R_0 \sim 1\text{--}2$  m), high-field ( $B_0 \sim 8\text{--}13$  T) tokamak ignition experiments.

---

\*Research sponsored by the Office of Fusion Energy, U.S. Department of Energy, under Contract No. DE-AC05-84OR21400 with Martin Marietta Energy Systems, Inc.



## 1. INTRODUCTION

There are many ways to model the detailed energy balance processes in burning plasmas. These include 0-D, 1-D, and 1½-D transport models, all of which rely on extrapolating the present tokamak data base to the burning plasma state. Steady-state global analyses have particular value because of the ease of calculating and presenting results in terms of global parameters. Multidimensional transport codes are, however, required for detailed assessment of nonlinear and spatially localized physical processes when the physics governing these processes can be specified in detail.

In this paper we present a systematic method of establishing ignition conditions and plasma operating regimes over large regions of parameter space under various physics assumptions using a simple, global model.<sup>1-4</sup> Specific features included in the model are: (1) plasma power balance considering various forms of ion ( $\chi_i$ ) and electron ( $\chi_e$ ) thermal diffusivities or global energy confinement times ( $\tau_E$ ); (2) consistent plasma profiles and geometry; (3) neoclassical enhancement of resistivity; (4) fast-alpha contribution to total pressure; (5) equilibrium plasma current model; and (6) various constraints imposed by equilibrium, stability, and confinement ( $q_\psi$ ,  $n_{\text{Murakami}}$ ,  $\beta_{\text{crit}}$ , etc.). In Sect. 2 the global plasma power balance is derived and a typical plasma parameter operating space is introduced. The physics models and constraints used to determine the plasma parameter operating space are summarized in Sect. 3. Contour analysis of ignition conditions and the plasma parameter operating regimes is presented in Sect. 4 for model confinement scalings. Nearly universal contour plots of ignition, auxiliary power, plasma heating and operating windows, ignition margins, etc., are found to exist for  $\chi_e$  (or  $\tau_{Ee}$ )  $\sim$  neo-Alcator-like and  $\chi_i \sim$  neoclassical scalings that are parameterized in terms of the Murakami density limit<sup>5</sup> and  $(aB_0^2/q_*)$ , the "figure-of-merit parameter," where  $q_*$  is the equivalent cylindrical safety factor ( $\lim_{\epsilon = r/R_0 \rightarrow 0} q_\psi = q_*$ ). Similar parameterization is also found for other confinement scalings.<sup>3</sup> These contour plots are then used to explore the potential physics design space, operating regimes, and plasma performance characteristics of small ( $R_0 \sim 1-2$  m), high-field ( $B_0 \sim 8-13$  T) tokamak ignition experiments that are currently being considered by the U.S. Tokamak Ignition Studies Design Teams.<sup>6-8</sup> Results are discussed in Sect. 5. Comparison of results with the 1½-D WHIST transport code<sup>9</sup> shows a reasonable agreement.

In all expressions, unless otherwise stated, mks units are used, with temperatures in kilo electron volts (keV), current in megamperes (MA), and power in megawatts (MW). When designated, densities are in units of  $10^{20} \text{ m}^{-3}$  ( $n_{20}$ ) and temperatures are in units of 10 keV ( $T_{10}$ ).

## 2. GLOBAL POWER BALANCE

The flux-surface-averaged energy balance equations for the electrons and the ions, when combined, can be written as

$$\frac{\partial}{\partial t} \left[ \frac{3}{2} n_e k T_e + \frac{3}{2} n_i k T_i \right] = \frac{1}{V'(\rho)} \frac{\partial}{\partial \rho} \left[ A(\rho) \left( n_e \chi_e \frac{\partial k T_e}{\partial \rho} + n_i \chi_i \frac{\partial k T_i}{\partial \rho} \right) \right] - p_{\text{rad}} + p_\alpha + p_{\text{OH}} + p_{\text{aux}} , \quad (1)$$

where

$$\begin{aligned} \rho &= \text{radial coordinate that labels a flux surface,} \\ V(\rho) &= 2 \pi^2 R_0 \rho^2 \kappa = \text{plasma volume contained within a flux surface,} \\ V'(\rho) &= \partial V / \partial \rho, \\ A(\rho) &= V'(\rho) \langle (\nabla \rho)^2 \rangle = (2\pi)^2 R_0 \rho \kappa [(1 + \kappa^2) / 2\kappa^2], \\ \chi_e(\chi_i) &= \text{electron (ion) thermal diffusivity,} \\ n_e &= \sum n_j Z_j = n_{\text{DT}} + 2n_\alpha + Z n_Z = \text{electron density,} \\ n_i &= n_{\text{DT}} + n_\alpha + n_Z = \text{total thermal-ion density,} \\ n_{\text{DT}} &= n_{\text{D}} + n_{\text{T}} = \text{fuel-ion density,} \\ T_e(T_i) &= \text{electron (ion) temperature.} \end{aligned}$$

The expressions given for  $V(\rho)$  and  $A(\rho)$  assume concentric elliptic flux surfaces with elongation  $\kappa = b/a$ . Correction for triangularity  $\delta$  can be included, approximately, by replacing  $(1 + \kappa^2)$  with  $[1 + \kappa^2(1 + 2\delta^2)]$ .

In Eq. (1) only the conduction losses (the first term on the right-hand side) are considered. Convection losses are neglected. The expressions for the various power densities  $p$  (MW/m<sup>3</sup>) are as follows. The bremsstrahlung radiation is

$$p_{\text{rad}} \text{ (MW/m}^3\text{)} \simeq (5.3 \times 10^{-43}) n_e^2 Z_{\text{eff}} T_e^{1/2} = (1.68 \times 10^{-20}) n_{e20}^2 Z_{\text{eff}} T_{e10}^{1/2} , \quad (2)$$

where  $Z_{\text{eff}} = \sum n_i Z_i^2 / n_e$  is the effective ion charge,  $n_{20} = n / (10^{20} \text{ m}^{-3})$ , and  $T_{10} = T / (10 \text{ keV})$ . Cyclotron radiation and impurity-line radiation are ignored.

The alpha power density is

$$p_\alpha \text{ (MW/m}^3\text{)} = n_D n_T \langle \sigma v \rangle_{DT} E_\alpha$$

$$\approx 0.155 \left[ 4f_D(1 - f_D) f_{DT}^2 \right] n_{e20}^2 T_{i10}^8, \quad (3)$$

where  $E_\alpha = 3.52$  MeV,  $f_D = n_D/n_{DT}$ ,  $f_{DT} = n_{DT}/n_e$ , and  $\langle \sigma v \rangle_{DT}$  (fusion reaction-rate parameter), for the temperature ranges of interest, is approximated as

$$\langle \sigma v \rangle_{DT} \approx \left( 1.1 \times 10^{-22} \right) T_{i10}^s \text{ (m}^3\text{/s)} \begin{cases} s \sim 3 & 4 \text{ keV} < T_i < 10 \text{ keV} \\ s \sim 2 & 10 \text{ keV} < T_i < 20 \text{ keV} \end{cases}$$

for a 50:50 D-T plasma ( $f_D = 0.5$ ) with  $Z_{\text{eff}} \approx 1$ , the term in square brackets in Eq. (3) is unity. For  $Z_{\text{eff}} \approx 1.5$  with  $n_\alpha/n_e \approx 0.05$  and  $Z = 8$  (oxygen),  $f_{DT} \approx 0.84$ .

The ohmic power density is

$$p_{OH} \text{ (MW/m}^3\text{)} = 10^6 \eta_{\parallel} \text{ (\Omega}\cdot\text{m)} J^2 \text{ (MA/m}^2\text{)} = E_{\parallel} \text{ (V/m)} J \text{ (MA/m}^2\text{)}$$

$$\approx (5.22 \times 10^{-5}) \gamma_{NC} Z_{\text{eff}} \ln \Lambda J^2 / T_{e10}^{3/2}, \quad (4)$$

where  $J$  is the local current density,  $J = E_{\parallel}/\eta_{\parallel}$ ,  $E_{\parallel}$  is the electric field that drives the current, and the parallel resistivity is  $\eta_{\parallel} = \eta_s \gamma_{NC}$  with the Spitzer resistivity

$$\eta_s = (1.65 \times 10^{-9}) Z_{\text{eff}} \ln \Lambda / T_e^{3/2} \text{ (\Omega}\cdot\text{m)} \quad (5)$$

and the neoclassical trapped-particle enhancement factor (at low collisionality,  $\nu_{*e} < 1$ ),

$$\gamma_{NC} \approx \left[ 1 - 1.95(r/R_0)^{1/2} + 0.95(r/R_0) \right]^{-1}. \quad (6)$$

Here  $\ln \Lambda \simeq 38.2 - \ln (n_e^{1/2}/T_e) \sim 15\text{--}20$  is the Coulomb logarithm. The current density on axis is

$$\begin{aligned} J(0) &= \frac{2}{\mu_0} \frac{B_0}{q(0)R_0} \left( \frac{1 + \kappa^2}{2\kappa} \right) \text{A/m}^2 \\ &= \frac{5}{\pi} \frac{B_0}{q(0)R_0} \left( \frac{1 + \kappa^2}{2\kappa} \right) \text{MA/m}^2 , \end{aligned} \quad (7)$$

where  $q(0) = q_0$  is the safety factor on axis, typically  $q_0 \sim 1$ . Sawtooth oscillations are initiated when the on-axis safety factor drops below one. When the sawtoothing is suppressed,  $q(0) \sim 0.5\text{--}0.8$  is typically attained.

“Ignition” is defined as the self-sustaining plasma state in which the fusion power deposited in the plasma by the alpha particles ( $p_\alpha$ ) is sufficient to balance the plasma energy losses associated with all loss processes without any applied external power ( $p_{\text{aux}} = 0$ ). Ohmic ignition is a special case in that the ohmic heating power is intrinsic to the configuration and cannot be turned off. Thus, we define the ignition as  $p_\alpha + p_{\text{OH}} =$  the sum of all losses when  $p_{\text{aux}} = 0$ . The global ignition condition can be obtained by volume averaging the local energy balance equation, Eq. (1), over given plasma profiles. Typical profiles assumed are shown in Fig. 1. The density, temperature, current density, and  $q$  profiles are nearly flat inside the sawtooth region ( $0 < r < r_s$ ). Outside the sawtooth region ( $r_s < r < a$ ), profiles can be represented as parabolic or Gaussian, where a principle of profile consistency<sup>11</sup> can be applied to determine self-consistent relationships between various power or exponent coefficients. To provide simple analytic expressions, we choose the profiles in the form

$$X(\rho) = X_0(1 - \rho^2/a^2)^{\alpha_X} , \quad (8)$$

where  $X = n, T,$  or  $J$  and typically  $\alpha_n \sim 0.5\text{--}1.0$ ;  $\alpha_T \sim 1.0\text{--}1.5$ ; and  $\alpha_J = 3\alpha_T/2$ . Thus, the average density, density-averaged temperature, and current density are

$$\langle n \rangle = n_0/(1 + \alpha_n) , \quad (9a)$$

$$\langle T \rangle = \langle nT \rangle / \langle n \rangle = T_0(1 + \alpha_n)/(1 + \alpha_n + \alpha_T) , \quad (9b)$$

$$\langle J \rangle = J_0/(1 + \alpha_J) = J_0/(1 + 3\alpha_T/2) . \quad (9c)$$

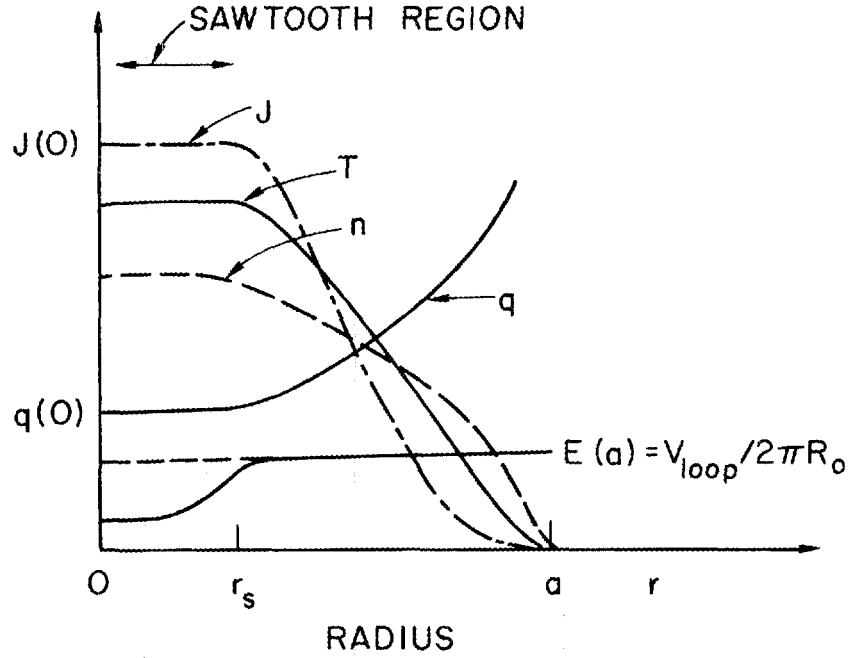


Fig. 1. Typical profiles for density ( $n$ ), temperature ( $T$ ), current density ( $J$ ), safety factor ( $q$ ), and electric field ( $E$ ).

In the remainder of this paper, unless otherwise stated, the average values are used without the angle brackets  $\langle \rangle$ .

The global power balance equation [obtained by multiplying Eq. (1) with  $dV = V'(\rho)d\rho$  and integrating over  $\rho$  with assumed profiles, Eq. (8)] is given by

$$\frac{\partial W}{\partial t} = -P_{\text{con}} - P_{\text{rad}} + P_{\alpha} + P_{\text{OH}} + P_{\text{aux}} . \quad (10)$$

Here, the total plasma energy is

$$W \text{ (MJ)} = W_e + W_i = 0.24 n_{e20} T_{e10} \left[ 1 + \frac{n_i}{n_e} \frac{T_i}{T_e} \right] V . \quad (11)$$

The power loss due to transport processes is

$$P_{\text{con}} \text{ (MW)} = 0.16 n_{e20} T_{e10} \left( \chi_e + \frac{n_i}{n_e} \frac{T_i}{T_e} \chi_i \right) \times \left[ \frac{4}{a^2} \left( \frac{1 + \kappa^2}{2\kappa^2} \right) g_c \left( \frac{\rho_*}{a}, \alpha_n, \alpha_T \right) \right] V . \quad (12)$$

The temperature gradients are evaluated at  $\rho_*/a < 1$ ,

$$g_c \left( \frac{\rho_*}{a}, \alpha_n, \alpha_T \right) = \alpha_T (1 + \alpha_n + \alpha_T) \left( \frac{\rho_*^2}{a^2} \right) \left( 1 - \frac{\rho_*^2}{a^2} \right)^{\alpha_n + \alpha_T - 1} . \quad (13)$$

For a given plasma profile  $(\alpha_n, \alpha_T)$ , the maximum value of  $g_c(\rho_*/a)$  occurs at  $\rho_*/a = (\alpha_n + \alpha_T)^{-0.5}$ . For example, for  $\alpha_n \simeq 0.5$  and  $\alpha_T \simeq 1.0$ ,  $\rho_*/a$  (at maximum)  $\simeq 0.82$  and  $g_c(\text{max}) \simeq 0.96$ . In Eq. (12)  $\chi_e$  and  $\chi_i$  are taken as average values. For  $Z_{\text{eff}} \sim 1.5$ , with  $Z \sim 8$  and  $n_\alpha/n_e \sim 0.05$ , we have  $n_i/n_e \sim 0.9$  and  $n_{DT}/n_e \sim 0.84$ .

In terms of the energy confinement times,

$$P_{\text{con}} \text{ (MW)} = 0.16 \int \frac{3}{2} \frac{n_{e20} T_{e10} + n_{i20} T_{i10}}{\tau_E} dV = 0.16 \int \frac{3}{2} \left( \frac{n_{e20} T_{e10}}{\tau_{Ee}} + \frac{n_{i20} T_{i10}}{\tau_{Ei}} \right) dV , \quad (14)$$

where  $\tau_{Ee}$ ,  $\tau_{Ei}$ , and  $\tau_E$  are the electron, ion, and total energy confinement times, respectively, due to the radial transport. From Eqs. (12) and (14),

$$\chi_j = \frac{3a^2}{8\tau_{Ej}} \left( \frac{2\kappa^2}{1 + \kappa^2} \right) g_\chi \left( \frac{\rho_*}{a}, \alpha_n, \alpha_T \right) \quad j = e, i , \quad (15)$$

where

$$g_x \left( \frac{\rho_*}{a}, \alpha_n, \alpha_T \right) = \left[ 1 - \left( 1 - \rho_*^2/a^2 \right)^{\alpha_n + \alpha_T + 1} \right] / g_c \left( \frac{\rho_*}{a}, \alpha_n, \alpha_T \right). \quad (16)$$

For typical profiles ( $\alpha_n \sim 0-1.0$ ,  $\alpha_T \sim 1.0-1.5$ ),  $g_x \sim 0.8-1.1$  for  $\rho_*/a \sim 0.6-0.8$ .

The radiation power is

$$\begin{aligned} P_{\text{rad}} (\text{MW}) &= (1.68 \times 10^{-2}) n_{e20}^2 T_{e10}^{1/2} Z_{\text{eff}} \frac{(1 + \alpha_n)^{3/2} (1 + \alpha_n + \alpha_T)^{1/2}}{(1 + 2\alpha_n + 0.5\alpha_T)} V \\ &= C_B n_{e20}^2 T_{e10}^{1/2} Z_{\text{eff}} V. \end{aligned} \quad (17)$$

For  $\alpha_n \sim 0-0.5$  and  $\alpha_T \sim 1.0$ ,  $C_B \sim (1.6-1.9) \times 10^{-2}$ .

The alpha power is

$$\begin{aligned} P_\alpha (\text{MW}) &= 0.155 \left[ 4f_D(1 - f_D)f_{DT}^2 \right] \frac{(1 + \alpha_n + \alpha_T)^s}{(1 + \alpha_n)^{s-2}(1 + 2\alpha_n + s\alpha_T)} n_{e20}^2 T_{e10}^s V \\ &= C_\alpha n_{e20}^2 T_{e10}^s V. \end{aligned} \quad (18)$$

For  $\alpha_n \simeq 0.5$ ,  $\alpha_T \simeq 1.0$ , and  $Z_{\text{eff}} \sim 1.5$  ( $f_{DT} \sim 0.84$ ,  $f_D = 0.5$ ),  $C_\alpha \simeq 0.22$  (for  $s \sim 3$ ).

The ohmic power is

$$\begin{aligned} P_{\text{OH}} (\text{MW}) &= (1.32 \times 10^{-4}) \frac{Z_{\text{eff}} \ln \Lambda}{T_{e10}^{3/2}} \frac{B_0^2}{q_0^2 R_0^2} \left( \frac{1 + \kappa^2}{2\kappa} \right)^2 \\ &\quad \times \left( \frac{1 + \alpha_n}{1 + \alpha_n + \alpha_T} \right)^{3/2} g_{\text{OH}} \left( \bar{\gamma}_{\text{NC}}, \alpha_T, r_s/a \right) V. \end{aligned} \quad (19a)$$

For typical profiles ( $\alpha_n \sim 0.5$ ,  $\alpha_T \sim 1.0$ ),  $g_{OH} \approx 0.5 \bar{\gamma}_{NC}$  where  $\bar{\gamma}_{NC}$  is the average (averaged over the temperature profile) neoclassical resistivity enhancement factor. For  $A = R_0/a \sim 2.5-3.5$ ,  $\bar{\gamma}_{NC} \approx 2.8-2.2$ . Thus,

$$P_{OH} \text{ (MW)} = C_{OH} Z_{\text{eff}} \bar{\gamma}_{NC} T_{e10}^{-3/2} (B_0^2/q_0^2 R_0^2) [(1 + \kappa^2)/2\kappa]^2 V . \quad (19b)$$

for  $\alpha_n \sim 0.5$  and  $\alpha_T \sim 1.0$ ,  $C_{OH} \approx 5.4 \times 10^{-4}$  for  $\ln \Lambda \approx 16$ .

The auxiliary power is assumed to be  $P_{\text{aux}} = \int p_{\text{aux}} dV \approx p_{\text{aux}} V$ . In general, the auxiliary power deposition profiles and requirements are functions of the plasma parameters ( $n$ ,  $T$ , etc.), especially in the case of neutral beam heating. Here, we consider radio-frequency-like heating using a Gaussian heating profile.

Substituting Eqs. (12)–(19) in Eq. (10),

$$\begin{aligned} F = \frac{1}{V} \frac{\partial W}{\partial t} = & -0.16 n_{e20} T_{e10} \left[ \chi_e + \frac{n_i}{n_e} \frac{T_i}{T_e} \chi_i \right] \left[ \frac{4}{a^2} \left( \frac{1 + \kappa^2}{2\kappa^2} \right) g_c \right] \\ & - C_B n_{e10}^2 T_{e10}^{1/2} Z_{\text{eff}} + C_\alpha n_{e20}^2 T_{e10}^s \\ & + C_{OH} Z_{\text{eff}} \bar{\gamma}_{NC} T_{e10}^{-3/2} \frac{B_0^2 \kappa^2}{q_0^2 R_0^2} \left( \frac{1 + \kappa^2}{2\kappa^2} \right)^2 + \frac{P_{\text{aux}}}{V} . \end{aligned} \quad (20)$$

In terms of the energy confinement times, the first term on the right-hand side of Eq. (20) can be replaced with

$$-0.24 n_{e20} T_{e10} \left[ \frac{1}{\tau_{Ee}} + \frac{(n_i/n_e)(T_i/T_e)}{\tau_{Ei}} \right] g_\chi g_c . \quad (21)$$

For  $\alpha_n = 0.5$ ,  $\alpha_T = 1.0$ , and  $Z_{\text{eff}} \approx 1.5$  ( $Z = 8$ ,  $n_\alpha/n_e = 0.05$ ),  $n_i/n_e \approx 0.9$ ,  $g_c \approx 0.96$ ,  $g_{\chi_-} \approx 0.98$ ,  $C_B \approx 1.7 \times 10^{-2}$ ,  $C_\alpha \approx 0.22$ ,  $C_{OH} \approx 5.4 \times 10^{-4}$  ( $\ln \Lambda/16$ ), and  $\bar{\gamma}_{NC} \approx 2.5$  ( $1 \pm 0.1$ ) for  $A \sim 2.5-3.25$ .

Depending on the various forms of the ion ( $\chi_i$ ) and electron ( $\chi_e$ ) thermal diffusivities (or the energy confinement times  $\tau_{Ei}$ ,  $\tau_{Ee}$ ), a wide range of tokamaks

could satisfy Eq. (20), subject to other physics constraints (e.g., beta limit, density limit,  $q_\psi$  limit, etc.), which are discussed in Sect. 3.

The characteristics of equilibrium are determined by  $F = 0$  ( $\partial W/\partial t = 0$ ). If  $\partial F/\partial T > 0$ , the average temperature will increase corresponding to thermal runaway. Contours of thermal runaway are obtained by setting  $F = \partial F/\partial T = 0$ . For  $F = 0$  ( $P_\alpha + P_{OH} + P_{aux} = P_{con} + P_{rad} \equiv P_{losses}$ ), we have either (1)  $P_\alpha + P_{OH} \geq P_{losses}$  for all  $T$ , so that  $P_{aux}$  is not required, or (2)  $P_\alpha + P_{OH} \geq P_{losses}$  for  $T_1 \leq T \leq T_2$ , so that  $P_{aux}$  is required to bridge the gap between  $T_1$  and  $T_2$ . The first case corresponds to an ohmic ignition. In the second case,  $P_{aux} = 0$  at  $T = T_1$  ( $= T_{OH}$ , ohmic equilibrium) and  $T = T_2$  ( $= T_{IGN}$ , ignition) and  $P_{aux} > 0$  for  $T_{OH} < T < T_{IGN}$ . Between these two temperatures,  $P_{aux} > P_{aux}(\max)$  is required, where  $P_{aux}(\max) = P_{aux}(T_*)$ ;  $\partial F/\partial T = \partial P_{aux}/\partial T = 0$  at  $T = T_*$ .

A typical plasma parameter operating space, in  $(\langle n \rangle, \langle T \rangle)$  space, is shown in Fig. 2, where equilibrium ( $F = 0$ ) contours for  $P_{aux} = 0$  (ohmic equilibrium and ignition) and  $\partial F/\partial T = \partial P_{aux}/\partial T = 0$  (thermal runaway) are shown. Also shown are the density limit ( $n_{max} \sim B_0/R_0$ , the Murakami limit) and the beta limit ( $\beta_{crit} \sim I/aB_0$ , the Troyon limit), as discussed in Sect. 3. In Fig. 2 the “heating window” is defined as the region where  $P_{aux} > 0$  [ $(\Delta T)_{heating} \equiv (\Delta T)_h = T_{IGN} - T_{OH}$ ]. The boundaries of the “operating window” (dotted region) are determined by confinement [ignition curve—solution to Eq. (20) for  $P_{aux} = 0$ ], the beta limit, and the density limit. Two special cases are: (1)  $(\Delta T)_h = 0$ —ohmic ignition, and (2)  $(\Delta T)_{op}$  [or  $(\Delta n)_{op}$ ] = 0—beta limit (or density limit) occurs before ignition. In the latter case, although there is no magnetohydrodynamic (MHD) stable access to ignition, there may be a driven ( $P_{aux} \neq 0$ ), high- $Q$  (energy gain) operation. If  $(\Delta T)_h \sim 0$ —few keV, the required auxiliary power is small ( $P_{aux} < P_{OH}$ ). If  $(\Delta T)_{op} \geq$  several keV [ $(\Delta n)_{op} \sim (0.2-0.5)n_{max}$ ], the margin for ignition is large. Here, the ignition margin  $M_I$  is defined as

$$M_I = (P_\alpha + P_{OH})/(P_{con} + P_{rad}) . \quad (22)$$

( $M_I = 1$  corresponds to the ignition condition.)

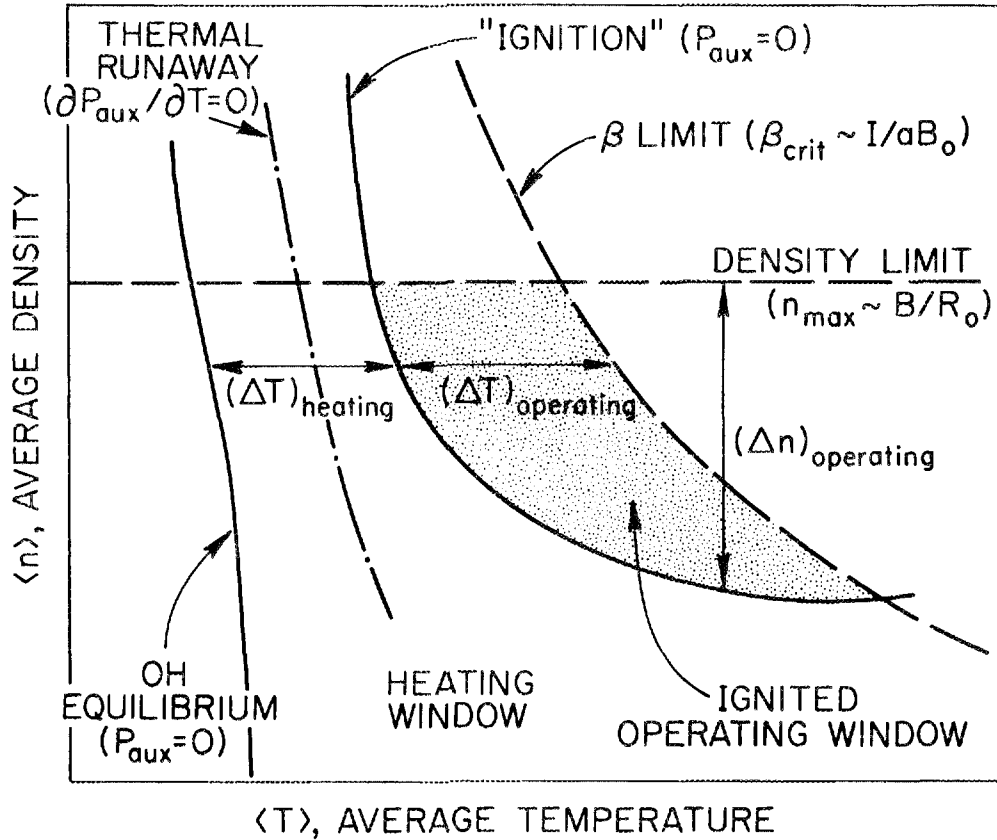


Fig. 2. Typical plasma parameter operating space showing equilibrium ( $\partial W/\partial t = 0$ ) contours for  $P_{aux} = 0$  (OH equilibrium and ignition) and  $\partial P_{aux}/\partial T = 0$  (thermal runaway) and the limits imposed on density ( $n_{max} \sim B_0/R_0$ , the Murakami limit) and total plasma beta ( $\beta < \beta_{crit} \sim I/aB_0$ , the Troyon limit). Heating window and operating window (dotted) are shown.

### 3. PHYSICS MODELS AND CONSTRAINTS

#### 3.1 Plasma Current

In general, MHD equilibrium calculations are carried out to accurately model the current (and, in turn, true MHD safety factor  $q_\psi$ ) dependence on plasma shape (elongation  $\kappa$ , triangularity  $\delta$ , etc.) and aspect ratio. A fit to these model equilibria can be characterized as

$$I \text{ (MA)} = \frac{5aB_0}{q_\psi} \frac{a}{R_0} \left[ \frac{1 + \kappa^2}{2} \right] f(\epsilon) = \frac{5a^2B_0}{q_*R_0} \left[ \frac{1 + \kappa^2}{2} \right], \quad (23)$$

where  $f(\epsilon)$  is a form factor that depends on aspect ratio ( $\epsilon = A^{-1} = a/R_0$ ), poloidal beta, plasma shape, etc. Typically,<sup>12</sup>  $f(\epsilon) \sim C_I/(1 - \epsilon^2)^2$  with  $C_I \sim 1.22-0.68$ . In Eq. (23),  $q_\psi = q_*f(\epsilon)$  and  $q_*$  is the equivalent cylindrical safety factor (i.e.,  $q_* = \lim_{\epsilon \rightarrow 0} q_\psi$ ). In Eq. (23), the triangularity correction can be included by replacing  $(1 + \kappa^2)$  with  $1 + \kappa^2(1 + 2\delta^2)$ , a reasonable approximation for  $\delta < 0.4$ ; thus,

$$q_* \approx \frac{5a^2B_0}{IR_0} \left[ \frac{1 + \kappa^2(1 + 2\delta^2)}{2} \right]. \quad (24)$$

### 3.2 Density Limit

In many tokamaks, the maximum density attainable in stable operation is seen to scale as  $B/R$ , known as the Murakami limit,<sup>5</sup>

$$n_{20} < n_{\text{mu}} = \nu_{\text{mu}} \frac{B_0}{q_*R_0}, \quad (25)$$

where  $\nu_{\text{mu}} \approx 1.5$  for ohmically heated plasmas, and  $\nu_{\text{mu}} \approx 2-3$  is found to be possible in some auxiliary heated plasmas. In calculations presented later, we define a normalized density as

$$m = \frac{\langle n_{20} \rangle}{n_{\text{mu}}} = \frac{\langle n_{20} \rangle q_* R_0}{\nu_{\text{mu}} B_0}, \quad \nu_{\text{mu}} = 1.5. \quad (26)$$

### 3.3 Beta Limit

A simple scaling law for the maximum volume-average beta that can be reached before the onset of ideal MHD instabilities is

$$\beta_{\text{crit}} \approx (0.03-0.04) \frac{I \text{ (MA)}}{a \text{ (m)} B_0 \text{ (T)}}. \quad (27)$$

This form of the beta limit, known as the Troyon limit,<sup>13</sup> has been observed experimentally and suggested by theoretical studies of macroscopic external kink<sup>13</sup> and

ideal-MHD ballooning instabilities.<sup>14</sup> This is a disruptive beta limit. Thus, the total plasma beta is taken as

$$\beta = \beta_e + \beta_i + \beta_{\text{fast-}\alpha} = (1 + \gamma_{f\alpha})(\beta_e + \beta_i) < \beta_{\text{crit}} , \quad (28)$$

where

$$\beta_e + \beta_i \simeq 0.4n_{e20}T_{e10} \left[ 1 + \frac{n_i}{n_e} \frac{T_i}{T_e} \right] / B_0^2 , \quad (29)$$

and  $\gamma_{f\alpha}$  is the ratio of the fast-alpha pressure to the plasma thermal pressure. In the temperature range of  $\langle T \rangle \simeq 6\text{--}16$  keV, the average pressure contribution from fast alphas is  $\simeq 5\text{--}25\%$  of the thermal plasma pressure. This fractional contribution, to lowest order, is independent of density,  $\gamma_{f\alpha} = \gamma_{f\alpha}(T)$ .

A beta limit expressible as  $I/aB_0$  can also be put into a form [see Eqs. (23) and (24)]

$$\beta_{\text{crit}} \sim \frac{I}{aB_0} \sim \frac{\epsilon f(\epsilon)}{q_\psi} \frac{1 + \kappa^2(1 + 2\delta^2)}{2} \sim \frac{1}{q_* A} \frac{1 + \kappa^2(1 + 2\delta^2)}{2} .$$

To maximize the total beta, the plasma must be shaped to maximize  $I/aB_0$  (i.e., small  $A$  and  $q_\psi$  and large  $\kappa$  and  $\delta$ ). Although low values of  $q_\psi$  are desirable, to achieve low disruptivity  $q_\psi$  is commonly limited to the range  $q_\psi > 2.6$ .

Substituting Eq. (26) in Eq. (28) and using Eqs. (24) and (27) we get

$$\frac{aB_0}{T_{10}} = 7.6\text{m} \left( 1 + \gamma_{f\alpha} \right) \left[ \frac{2}{1 + \kappa^2} \right] . \quad (30)$$

Thus, in  $(m = \langle n \rangle / n_{\text{mu}}, \langle T \rangle)$  space,  $\beta = \beta_{\text{crit}}$  contours correspond to contours of constant  $aB_0$ . For high-field, compact ignition experiments,<sup>6-8</sup> a typical parameter range is  $aB_0 \sim 4.5\text{--}5.0$  (mT). The average maximum toroidal beta contours,  $\beta_{\text{tot}} = \beta_{\text{crit}} / (1 + \gamma_{f\alpha}) \sim T_{10} / aB_0$ , are shown in Fig. 3. The contribution from fast alphas  $\gamma_{f\alpha}$  is included in the total pressure.  $\beta = \beta_{\text{crit}}$  on the curves,  $\beta > \beta_{\text{crit}}$  above the curves, and  $\beta < \beta_{\text{crit}}$  (stable operation) below the curves.

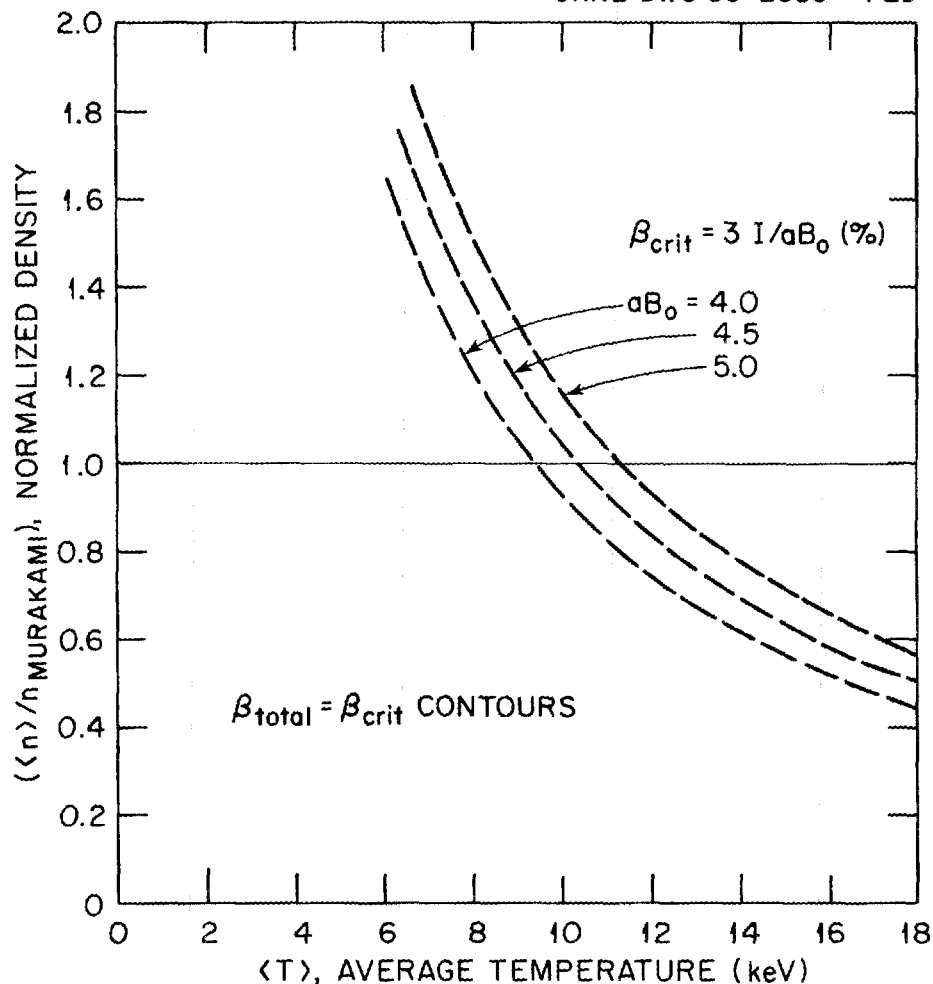


Fig. 3. Contours of maximum attainable toroidal beta, including fast-fusion-alpha pressure contribution, for several values of  $aB_0$ .  $\beta = \beta_{\text{crit}} = 3I/aB_0$  on the curves,  $\beta > \beta_{\text{crit}}$  above the curves, and  $\beta < \beta_{\text{crit}}$  below the curves. Here  $\beta = \beta_{\text{tor}} + \beta_{\text{fast-}\alpha}$  is the total beta with  $\beta_{\text{tor}} = \beta_e + \beta_i$ .

### 3.4 Confinement Models

**Ion confinement.** The observed ion confinement is generally consistent with the predictions of the neoclassical theory. The expression for  $\chi_i$ , including finite aspect ratio correction, is given by the Chang-Hinton formula.<sup>15</sup> In low collisionality (banana regime),

$$\chi_{iCH} \text{ (m}^2/\text{s)} \simeq (2 \times 10^{-2}) K_2^* \frac{n_{e20} Z_{\text{eff}} q_*^2}{\epsilon^{3/2} T_{i10}^{1/2} B_0^2} \left( \frac{2}{1 + \kappa^2} \right), \quad (31)$$

where

$$K_2^* = (0.66 + 1.88\epsilon^{1/2} - 1.54\epsilon)(1 + 1.5\epsilon^2), \quad \epsilon = r/R_0. \quad (32)$$

A corresponding expression for  $\tau_{Ei}$  can be obtained from Eq. (15).

**Electron confinement.** The scaling laws for  $\chi_e$  or  $\tau_{Ee}$  are empirical (or semi-empirical) both for ohmic and auxiliary heated plasmas. A large body of such scalings exists; a few of these are summarized here. Because most of the work on empirical scaling laws has focused on finding scalings for the global confinement time  $\tau_E$  or the electron energy confinement time  $\tau_{Ee}$ , we present the expressions for  $\tau$ . A corresponding expression for the average thermal diffusivity can easily be obtained from Eq. (15).

The simplest scaling law that describes both the low-density and high-density regimes of small and large ohmic tokamaks, referred to as the “neo-Alcator,”<sup>16</sup> is

$$\tau_{NA} \simeq 0.07 n_{20} a R_0^2 q_* , \quad (33)$$

which is used for  $\tau_E$  or  $\tau_{Ee}$  (or total  $\tau_{\text{gross}}$ ). The thermal diffusivity is then

$$\chi_{NA} \simeq \frac{0.3a^2}{\tau_{NA}} \left( \frac{2\kappa^2}{1 + \kappa^2} \right) \simeq \frac{4.3a}{n_{20} R_0^2 q_*} \left( \frac{2\kappa^2}{1 + \kappa^2} \right). \quad (34)$$

A deterioration of confinement is observed when strong auxiliary heating is applied. The data from most experiments indicate an L-mode (poor-confinement) scaling of the form

$$\tau_E \propto I^{(1-1.5)} \left[ P^{-(1/3-2/3)} \text{ or } b + a/P \right], \quad (35)$$

where  $P$  is, in general, the total power ( the sum of the ohmic and absorbed beam power). Under specific conditions, it may be possible to recover some (or all) of the degradation (H-mode). Typically,  $\chi_e(\text{L-mode}) \simeq (2-4) \chi_e(\text{OH})$ , and  $\chi_e(\text{H-mode}) \leq 0.5 \chi_e(\text{L-mode})$ .

A general trend in scalings with auxiliary heating is that confinement improves with plasma current. One such simple scaling, referred to as the "Mirnov" or "GMS" scaling<sup>17</sup> is

$$\tau_{EM}^L \approx 0.15 a I \kappa^{1/2}, \quad \text{or} \quad \chi_{EM}^L \approx \frac{2a}{I \kappa^{1/2}} \left( \frac{2\kappa^2}{1 + \kappa^2} \right) \quad (36)$$

for an L-mode, and  $\tau_{EM}^H \approx (2-3) \tau_{EM}^L$  for an H-mode.

An example for degradation of confinement with increasing power is an L-mode scaling of Kaye and Goldston,<sup>18</sup>

$$\tau_{EKG}^L \approx 0.056 I^{1.24} P^{-0.58} R^{1.65} a^{-0.49} \kappa^{0.28} n_{20}^{0.26} B_0^{-0.09} A_i^{0.5}, \quad (37)$$

where  $P$  is in MW,  $I$  is in MA, and  $A_i$  is the ion atomic mass number. By taking  $P = 0.24 n_{20} T_{10} V / \tau_{Ee}$  and  $A_i \sim 2.5$  for a D-T plasma,

$$\tau_{EKG}^L \approx 3.65 \times 10^{-4} \frac{I^{2.95} R_0^{2.55}}{n_{20}^{0.76} T_{10}^{1.38} a^{3.93} B_0^{0.21} \kappa^{0.71}} \quad (38)$$

In general, Eq. (38) leads to rather pessimistic predictions when extrapolated to future ignition experiments (and/or reactors).

#### 4. CONTOUR ANALYSIS OF IGNITION CONDITIONS AND PLASMA OPERATING REGIMES

The global power balance equation [Eq. (20)] described in Sect. 2, subject to the physics models and constraints given in Sect. 3, could be used to generate contour plots of ignition, auxiliary power requirements, plasma heating and operating windows, and maximum attainable ignition margins (within the operating window) in density-temperature space.

For many of the confinement scalings, Eq. (20) can be solved analytically, especially for scaling laws with  $\tau_E \sim n^x T^y L^z \dots$ , where  $L$  is a characteristic scale length ( $L^3 \sim aR^2$  for neo-Alcator-like scaling,  $L^2 \sim a^2$  for neoclassical scaling, etc.) and  $x, y, z, \dots$  are multiples of  $1/2$ . For arbitrary exponential powers, approximate solutions (analytically) are possible by considering the leading-order terms in appropriate temperature and density ranges. Details of these calculations are given in Ref. 3. Here, we consider two examples:

1. Global confinement scaling–Neo-Alcator-like

- a.  $\tau_{\text{gross}} \sim \tau_{\text{neo-Alcator}}$ —all losses (rad + con) included in the scaling
- b.  $\tau_E \sim \tau_{\text{neo-Alcator}}$ —global energy confinement due to conduction

2. Combined neoclassical ion and neo-Alcator electron scalings:

$$\begin{aligned} \chi_i &= f_{ix} \chi_{iCH}, & f_{ix} &= 1-3 \\ \chi_e &= f_{ex} \chi_{NA}, & f_{ex} &= 1-2 \end{aligned}$$

To normalize the calculations, we set:  $\alpha_n = 0.5$ ,  $\alpha_T = 1.0$ ,  $\kappa \simeq 1.6$ ,  $\delta \simeq 0.2$ ,  $T_i/T_e \simeq 1.0$ ,  $q_\psi \simeq 2.6$ , and  $Z_{\text{eff}} \simeq 1.5$  with  $Z = 8$  and  $n_o/n_e = 0.05$ . Using these selections,  $n_i/n_e = 0.9$ ,  $n_{DT}/n_e = 0.84$ , and  $q_* \simeq 2.0$  ( $1 \mp 0.05$ ) for  $A \simeq 3.0 \mp 0.5$ . Note that  $q_*(a)/q(0) = 1 + 3\alpha_T/2 = 2.5$  (for the assumed current profile  $\alpha_j = 3/2\alpha_T$ ), thus,  $q_0 = q(0) \simeq 0.8$  is possible if sawtoothing does not occur. Calculations are presented both for  $q(0) = 1.0$  and  $q(0) = 0.8$ .

#### 4.1 Ignition Contours

**4.1.1 Neo-Alcator-like global confinement scaling. Example 1(a):** First, we consider a simple case and assume  $\tau_{\text{gross}} \sim \tau_{NA}$ . Defining  $\tau_{\text{gross}} = W/P_{\text{losses}} = (W_e + W_i)/(P_{\text{rad}} + P_{\text{con}})$  and taking  $\tau_{\text{gross}} = \tau_{NA} (= 0.07n_{20}aR_0^2q_*)$ , the ignition requirement [Eq. (20) with  $F = 0$  and  $P_{\text{aux}} = 0$ ] is

$$6.52 \frac{T_{10}}{aR_0^2q_*} \leq 0.22n_{e20}^2T_{10}^3 + 10^{-3}\bar{\gamma}_{NC} \frac{B_0^2}{q_0^2R_0^2} T_{10}^{-3/2}. \quad (39)$$

In terms of normalized density [Eq. (26)], this can be rewritten as

$$6.52 T_{10} \leq 0.495 m^2 (aB_0^2/q_*) T_{10}^3 + (10^{-2}/q_0^2) (aB_0^2/q_*) T_{10}^{-3/2},$$

or

$$a_1 T_{10} - a_2 m^2 T_{10}^3 - a_3 T_{10}^{-3/2} = 0, \quad (40)$$

where  $\bar{\gamma}_{NC} \simeq 2.5$  ( $1 \pm 0.1$ ) is used, and a reasonable value for  $A \simeq 3 \mp 0.5$ . Note that it is easier to satisfy Eq. (40) for large values of  $(aB_0^2/q_*)$ . Here we define  $(aB_0^2/q_*)$  to be a “figure-of-merit parameter.” [Since  $\tau \sim naR_0^2q_*$  and  $n_{\text{max}} \sim B_0/q_*R_0$ , then  $(n\tau)_{\text{max}} \sim (aB_0^2/q_*)$ .] [For  $T > 10$  keV,  $a_2 T_{10}^3 \rightarrow a_2 T_{10}^2$  in Eq. (39) or (40).]

Solutions to  $F = 0$  [Eq. (40)] and  $\partial F/\partial T = \partial P_{\text{aux}}/\partial T = 0$  ( $a_1 - 3a_2 m^2 T_{10}^2 + 1.5a_3 T_{10}^{-5/2} = 0$ ) are as follows: ohmic equilibrium temperature is

$$(T_{10})_{\text{OH}} = (a_3/a_1)^{0.4} \simeq 0.075(aB_0^2/q_*)^{0.4}/q_0^{0.8} . \quad (41)$$

$P_{\text{aux}} = \partial P_{\text{aux}}/\partial T = 0$  at  $m_*$ ,  $T_*$ , where

$$(T_{10})_* = (9a_3/4a_1)^{0.4} \simeq 0.104(aB_0^2/q_*)^{0.4}/q_0^{0.8} \quad (42a)$$

$$m_*^2 = \frac{a_1(T_{10})_* - a_3(T_{10})_*^{-3/2}}{a_2(T_{10})_*^3} , \quad (42b)$$

which gives

$$m_* \simeq 26.12q_0^{0.8}/(aB_0^2/q_*)^{0.9} \simeq 0.16(T_{10})_*^{-9/4}/q_0 . \quad (42c)$$

In Fig. 4 steady-state ignition/ohmic equilibrium contours ( $P_{\text{aux}} = 0$ ) for various values of  $aB_0^2/q_*$  are plotted in  $(\langle n \rangle/n_{\text{mu}}, \langle T \rangle)$  space for  $q(0) = 1.0$  and  $0.8$ .  $\beta = \beta_{\text{crit}}$  contours (Fig. 3) for  $aB_0 = 4.5$  and  $5$  are also superimposed. For a given  $aB_0^2/q_*$ ,  $P_{\text{aux}} = 0$  on the curve,  $P_{\text{aux}} > 0$  under the curve, and  $P_{\text{aux}}$  above the curve. The plasma operating window (Fig. 2) for a given  $aB_0^2/q_*$  is the region above the ignition curve (corresponding to a given  $aB_0^2/q_*$ ) and below the  $\beta = \beta_{\text{crit}}$  and  $m \equiv \langle n \rangle/n_{\text{mu}} < 1$  lines. As can be seen, ohmic ignition with  $m < 1$  is possible (under the scaling assumption  $\tau_{\text{gross}} = \tau_{\text{NA}}$ , where all losses are included in the scaling) for devices with  $(aB_0^2/q_*) > 37q_0^{8/9}$ . For example, for  $q(0) = 1$ , this corresponds to  $(aB_0^2/q_*) > 37$ ; for  $q(0) = 0.8$ ,  $(aB_0^2/q_*) > 30.3$ ; and for  $q(0) = 0.5$ , the required value for the figure-of-merit parameter is  $(aB_0^2/q_*) \gtrsim 20$ .

**Example 1(b):** The case presented in the previous example is a very optimistic one. The bremsstrahlung radiation is the irreducible minimum loss. Here we will include the radiation losses and assume  $\tau_E = \tau_{\text{NA}}$  ( $\tau_E = W/P_{\text{con}}$ ). The ignition requirement is then

$$a_1 T_{10} + a_4 m^2 T_{10}^{1/2} - a_2 m^2 T_{10}^3 - a_3 T_{10}^{-3/2} = 0 , \quad (43)$$

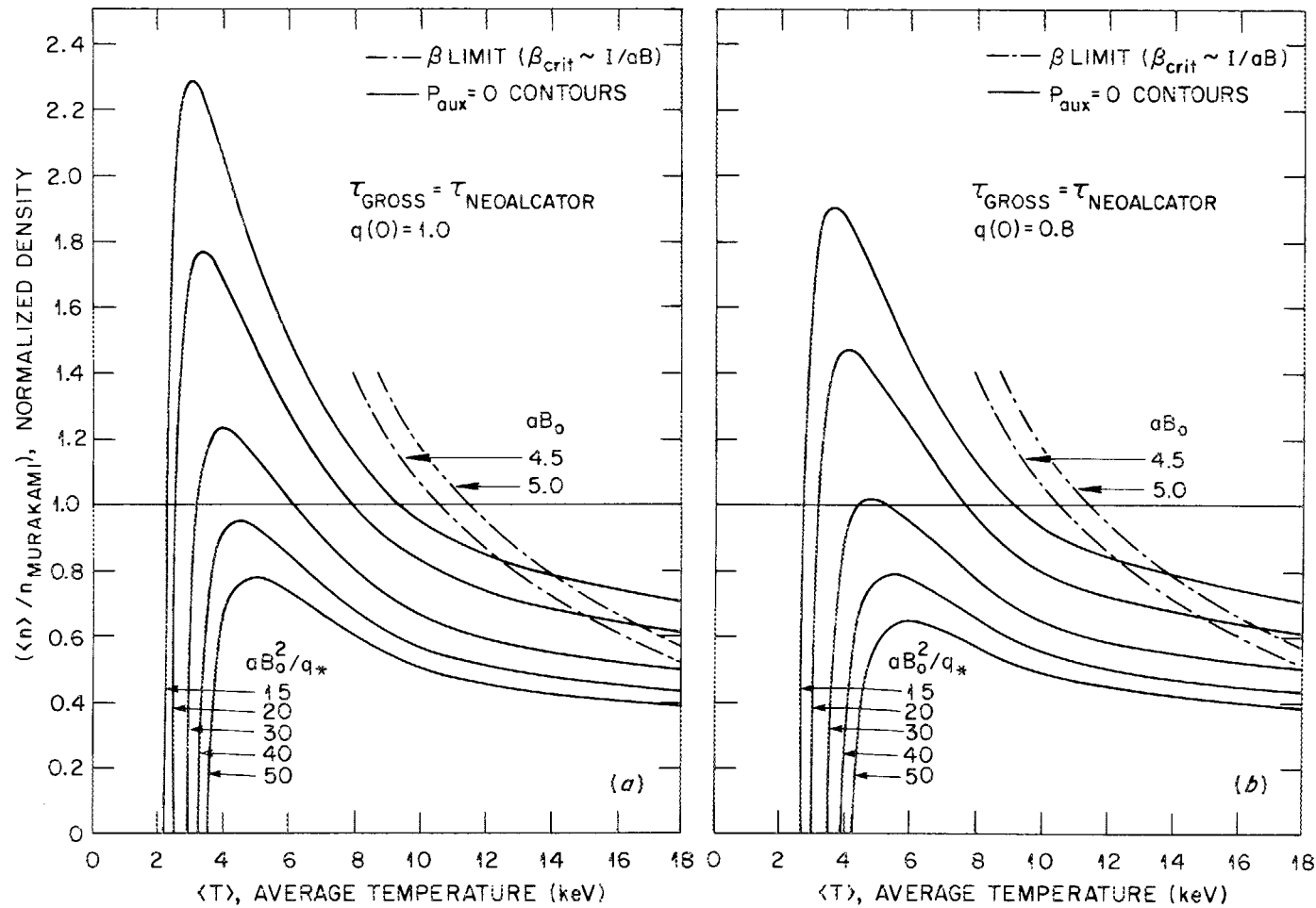


Fig. 4. Steady-state  $P_{\text{aux}} = 0$  contours for values of  $aB_0^2/q_*$  for (a)  $q(0) = 1.0$  and (b)  $q(0) = 0.8$ .  $\beta = \beta_{\text{crit}}$  contours are superimposed for  $aB_0 = 4.5$  and 5. **Confinement model:**  $\tau_{\text{gross}} = \tau_{\text{neo-Alcator}}$  (all losses, conduction + radiation, included in the scaling). Requirements for ohmic ignition at a given  $m = \langle n \rangle / n_{\text{mu}}$ , relative size of heating and operating windows, and optimal path (minimum  $P_{\text{aux}}$ ) to ignition can easily be determined from the figure. For  $m \leq 1$ , ohmic ignition is possible if (a)  $aB_0^2/q_* > 37$  for  $q(0) = 1.0$  and (b)  $aB_0^2/q_* > 30.3$  for  $q(0) = 0.8$ .

where  $a_4 = 5.7 \times 10^{-2} (aB_0^2/q_*)$ . Solutions for  $F = 0$  and  $\partial F/\partial T = \partial P_{\text{aux}}/\partial T = 0$  are as follows:

$$(T_{10})_{\text{OH}} \approx (a_3/a_1)^{0.4}, \quad (44a)$$

$$(T_{10})_{*1,2} = \left[ \frac{B \mp \sqrt{B^2 - 4AC}}{2A} \right]^{0.4}, \quad (44b)$$

$$m_{*1,2}^2 = \frac{a_1(T_{10})_{*1,2} - a_3(T_{10})_{*1,2}^{-3/2}}{a_2(T_{10})_{*1,2}^3 - a_4(T_{10})_{*1,2}^{1/2}}, \quad (44c)$$

where  $A = a_1 a_2 > 0$ ,  $B = (9a_2 a_3 - a_1 a_4)/4$  (should be negative for physical solutions), and  $C = a_3 a_4$ .  $T_{*1} = T_{*2}$  if  $B^2 - 4AC = 0$  (note that at this point  $P_{\text{OH}} = P_\alpha = P_{\text{con}} = P_{\text{rad}}$ ), which corresponds to minimum OH ignition condition).

Steady-state ignition contours ( $P_{\text{aux}} = 0$ ) for various values of  $aB_0^2/q_*$  are plotted in Fig. 5. Comparison of Figs. 4 and 5 clearly indicates the importance of the radiation term. For a given  $aB_0^2/q_*$ ,  $P_{\text{aux}} = 0$  on the designated curves. If  $B^2 - 4AC < 0$ ,  $P_{\text{aux}} > 0$  is required to bridge the gap between ohmic equilibrium and ignition branches. For large enough  $aB_0^2/q_*$ ,  $B^2 - 4AC$  can be made positive. In this case there exists a density window ( $m_{*1} < m < m_{*2}$ ) where  $P_{\text{aux}} < 0$  and ohmic ignition is accessible. These features can be seen from Fig. 5. Restricting density to the Murakami limit ( $m = 1$ ), ohmic ignition is possible for devices with  $aB_0^2/q_* > 57$  for  $q(0) = 1$  and  $> 41$  for  $q(0) = 0.8$ . These types of requirements for ohmic ignition translate into the requirements of  $B_0 \sim 12\text{--}14$  T,  $a \sim 0.4\text{--}0.6$  m for  $q_\psi \sim 2.6$  ( $q_* \leq 2$ ).

**4.1.2 Combined neoclassical ion and neo-Alcator electron scalings.** Taking  $\chi_e = f_{ie}\chi_{\text{NA}}$  and  $\chi_i = f_{ix}\chi_{\text{CH}}$ , where  $\chi_{\text{NA}}$  and  $\chi_{\text{CH}}$  are given by Eqs. (34) and (31), respectively, with  $f_{ex} \sim 1\text{--}2$  and  $f_{ix} \sim 1\text{--}3$ , the ignition requirement is

$$b_1 T_{10} + b_4 m^2 T_{10}^{1/2} - b_2 m^2 T_{10}^3 - b_3 T_{10}^{-3/2} = 0, \quad (45)$$

where  $b_1 = 3.43 f_{ex}$ ,  $b_4 = a_4 + (3.2 \times 10^{-2}) f_{ix} (R_0/a)^{3/2} (q_*/a) K_2^* \approx a_4 + f_{ix}$ ,  $b_2 = a_2$ ,  $b_3 = a_3$ . Here we approximated  $(R_0/a)^{3/2} (q_*/a) K_2^* \approx 31.5$ , which is reasonable ( $\pm 10\%$ ) for  $A \sim 2.5\text{--}3.5$ ,  $q_\psi \sim 2.6$ . Equation (45) is similar to

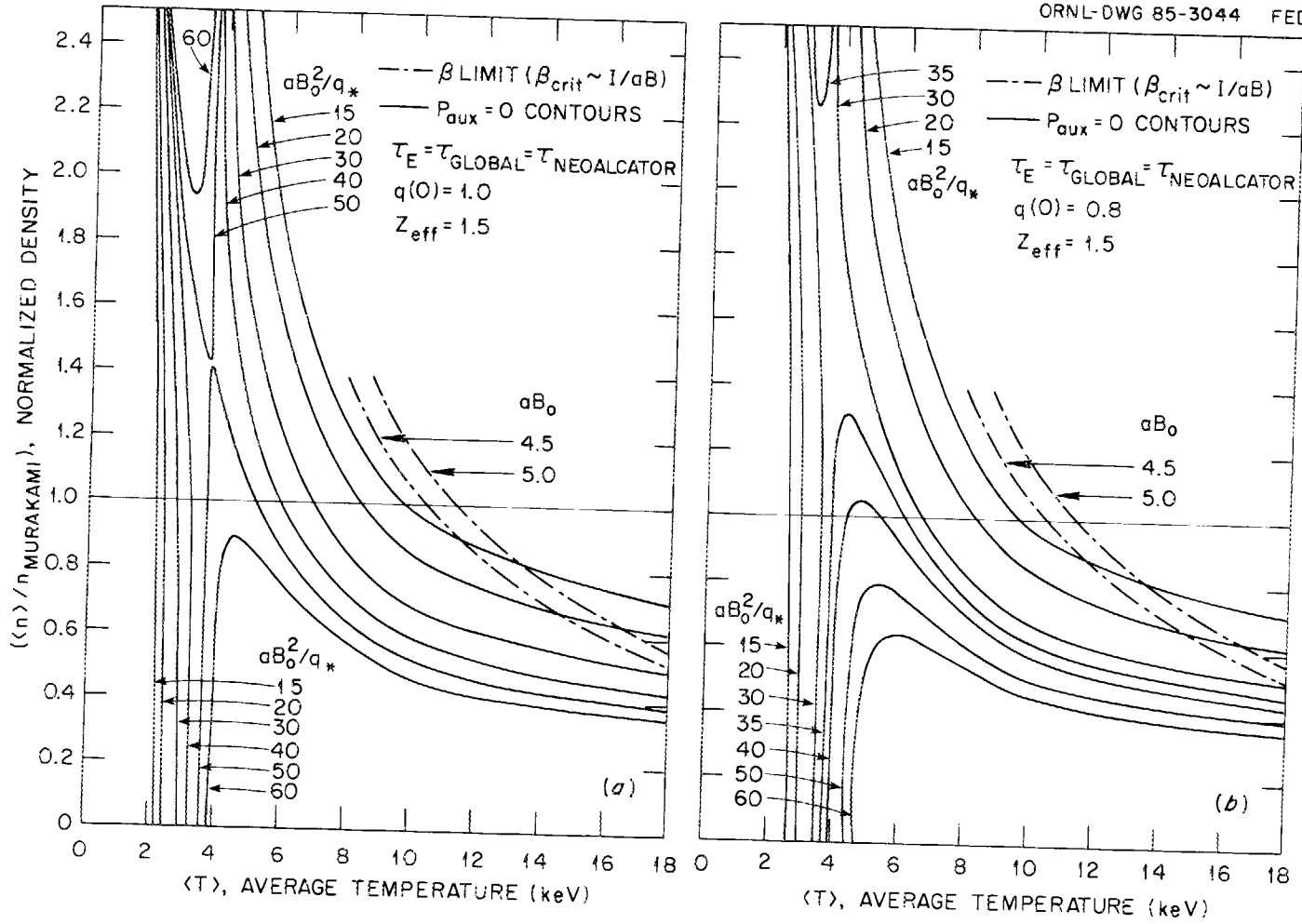


Fig. 5. Same as Fig. 4 except the confinement model is  $\tau_E = \tau_{neo-Alcator}$ , where  $\tau_E = W/P_{con}$  is the global energy confinement time. For  $m \leq 1$ , ohmic ignition is possible if (a)  $aB_0^2/q_* > 57$  for  $q(0) = 1.0$  and (b)  $aB_0^2/q_* > 41$  for  $q(0) = 0.8$ .

Eq. (43). Ignition contours are shown in Fig. 6 for  $f_{ex} = 1$  and  $f_{ix} = 1$  and 3. Results shown are for  $q(0) = 0.8$ . Comparison of Figs. 5 and 6 clearly indicates the role of ion conduction. We see that there is an optimal density path to ignition in  $(n, T)$  space where the  $(\Delta T)_h$  window (and  $P_{aux}$ ) is minimum. [This optimal density path resembles the ‘‘Cordey pass’’ for neutral beam heating.<sup>19</sup>] The optimal density along this path is bounded on the high-density side by ion neoclassical losses and on the low-density side by electron thermal conduction. For a given device, the ignition and ohmic equilibrium contours obtained from the POPCON (Plasma Operation CONtours) analysis of the 1/2-D WHIST transport code<sup>9</sup> are very much in agreement with the results shown in Fig. 6. Comparisons of the results of global and 1/2-D transport calculations are given in Refs. 2 and 4. This is not too surprising because the global model described here includes detailed enough physics and profile information and because the expressions for  $\chi_e$  used in 1-D or 1/2-D codes are deduced from the empirical (not theoretical) scaling laws (in most cases for  $\tau_{Ec}$ , not  $\chi_e$ ) obtained in terms of global plasma parameters.

Returning to Fig. 6 we see that the ohmic ignition is possible if  $(aB_0^2/q_*) > 37$  for  $f_{ix} = 1$  and  $> 55$  for  $f_{ix} = 3$ , both for  $q(0) = 0.8$ . The optimal density path is at  $m_* \sim 0.85$  ( $f_{ix} = 1$ ) or  $\sim 0.65$  ( $f_{ix} = 3$ ).

The ignition requirements become more stringent when electron losses are doubled ( $f_{ex} = 2$ ). In this case, devices with  $(aB_0^2/q_*) < 20$  reach their density and beta limit before they achieve ignition (i.e., operating window is zero).

Solutions for  $F = 0$  and  $\partial F/\partial T = \partial P_{aux}/\partial T = 0$  are in the same form as Eq. (44). Note that at  $T_{*1} = T_{*2}$  (saddle point or optimal path), we now have  $P_\alpha = P_{OH} = P_{con,e} = P_{rad} + P_{con,i}$ , which occurs at  $m < 1$  (see Fig. 6).

## 4.2 Heating and Operating Windows

As can be seen from the contour plots generated (Figs. 3–6), devices with large  $aB_0^2/q_*$  have favorable heating and operating windows. As  $aB_0^2/q_*$  increases, the  $(\Delta T)$  heating window decreases, leading to smaller auxiliary power requirements and larger margins against uncertainties associated with confinement scalings, heating, etc. Also as  $aB_0^2/q_*$  increases,  $(\Delta n)$  and  $(\Delta T)$  operating windows increase, allowing larger margins for ignition. Moreover, a large  $(\Delta T)$  [and  $(\Delta n)$ ] operating window allows one to separate the physics of ignition and burning plasma properties from those associated with the beta (and density) limits. Figure 7 shows the variation of these heating and operating windows with  $aB_0^2/q_*$  for two of the confinement scalings considered, corresponding to Figs. 5 and 6. Note that the assumption of  $q(0) = 1.0$  or  $q(0) = 0.8$  has very little or no impact on  $(\Delta T)_{op}$  for  $aB_0^2/q_* < 25$  (because the ohmic heating is negligible or small around  $T_{IGN}$  corresponding to these cases). However, the size of the heating window is very sensitive to the  $q(0)$  assumption, especially for  $aB_0^2/q_* > 25$ .

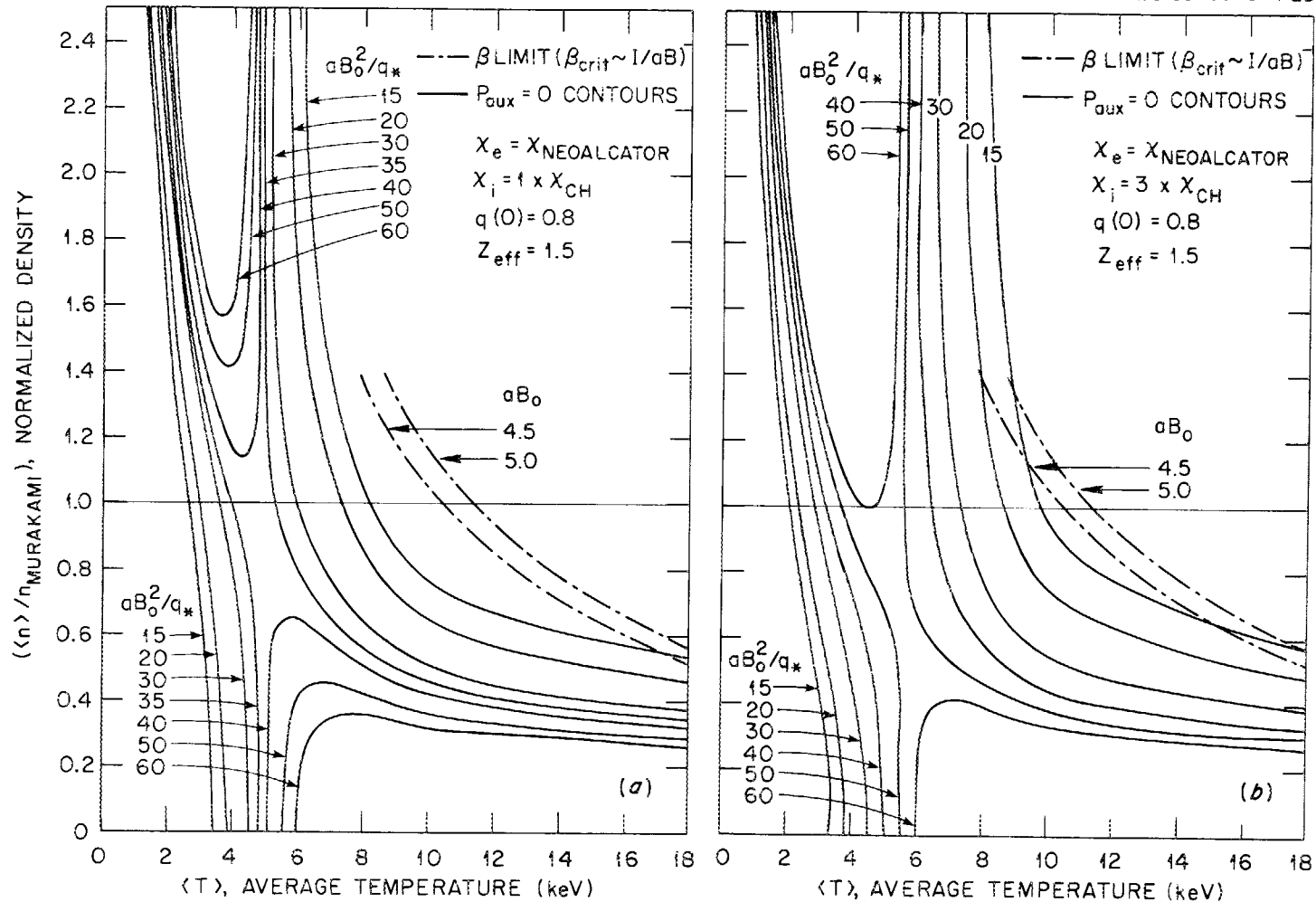


Fig. 6. Same as Fig. 4 except the confinement model is (a)  $\chi_e = \chi_{\text{neo-Alcator}}$  and  $\chi_i = 1 \times \chi_{\text{Chang-Hinton}}$  and (b)  $\chi_e = \chi_{\text{neo-Alcator}}$  and  $\chi_i = 3 \times \chi_{\text{Chang-Hinton}}$ ;  $q(0) = 0.8$  for both cases. Optimal density path to ignition (narrowest  $\Delta T$  heating window) is clearly evident and occurs at (a)  $\langle n \rangle \approx 0.85 n_{\text{mu}}$  and (b)  $\langle n \rangle \approx 0.65 n_{\text{mu}}$ . Along this optimal path, ohmic ignition is possible if (a)  $aB_0^2/q_* > 37$  and (b)  $aB_0^2/q_* > 55$ .

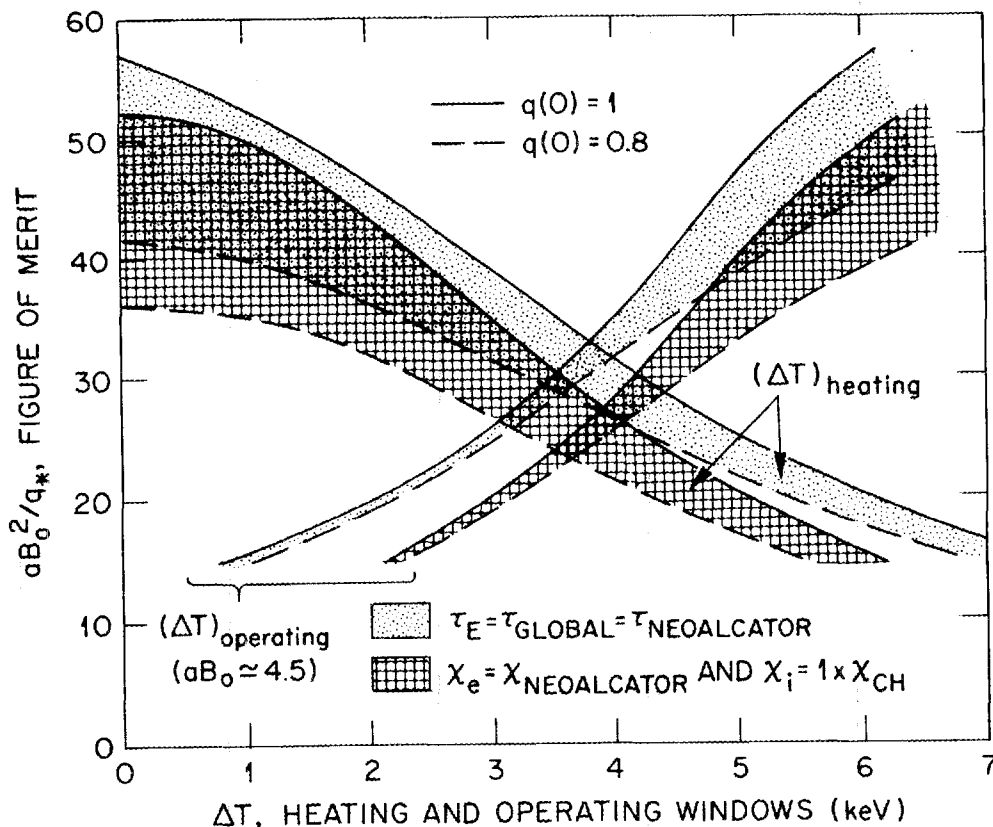


Fig. 7. Figure of merit ( $aB_0^2/q_*$ ) vs  $(\Delta T)$  heating and operating windows for  $\tau_E = \tau_{\text{neo-Alcator}}$  (dotted) and  $\chi_e = \chi_{\text{neo-Alcator}}$  plus  $\chi_i = \chi_{\text{Chang-Hinton}}$  (cross-hatched). Here  $(\Delta T)_{\text{op}}$  is measured at the Murakami limit (not along the optimal path) taking  $aB_0 \approx 4.5$  as an average value.

### 4.3 Ignition Margin

The ignition margin is defined by Eq. (22),  $M_I = (P_\alpha + P_{\text{OH}})/(P_{\text{con}} + P_{\text{rad}})$ , which can easily be evaluated for a given confinement scaling subject to the density- and beta-limit considerations. Note that  $M_I = M_I(Tn\tau) = M_I(\beta B_0^2 \tau)$ . Within the plasma operating window, the maximum margin for ignition is obtained where  $\langle n \rangle = n_{\text{mu}}$  ( $m = 1$ ) and  $\beta = \beta_{\text{crit}}$ . This is true for any confinement scaling of the form  $\tau_E \sim KnT^y$  with  $y > -1$ , where  $K$  contains the dependence of  $\tau_E$  on any parameter other than  $n$  and  $T$ . (For neo-Alcator scaling,  $y = 0$ ; for neoclassical scaling,  $y = 0.5$ , etc.) As an example, we consider  $\chi_e = 1 \times \chi_{\text{NA}}$  and  $\chi_i = 3 \times \chi_{\text{CH}}$  with  $q(0) = 1.0$  and  $s = 2$ ; then

$$M_I = \frac{aB_0^2}{q_*} \frac{0.495m^2T_{10}^2 + 10^{-2}T_{10}^{-3/2}}{3.43T_{10} + m^2[3 + (5.7 \times 10^{-2})(aB_0^2/q_*)]T_{10}^{1/2}} \quad (46)$$

Maximum value for  $M_I$  is at  $m = 1$  ( $\langle n \rangle = n_{\text{mu}}$ ) and  $T_{10} = T_{\text{crit}}$ , where  $T_{\text{crit}}$  corresponds to a temperature where  $\beta(n_{\text{mu}}) = \beta_{\text{crit}}$ ; [that is, see Eq. (30)],

$$(T_{10})_{\text{crit}} = aB_0 \left[ 7.6(1 + \gamma_{f\alpha}) \frac{2}{1 + \kappa^2(1 + 2\delta^2)} \right]^{-1} \\ = 0.25(aB_0)/(1 + \gamma_{f\alpha}) \approx 0.23aB_0 \quad (47)$$

For example, if  $aB_0^2/q_* \approx 20$  ( $a \sim 0.5$  m,  $B_0 \sim 9$  T,  $q_* \sim 2$ ), then  $aB_0 \sim 4.5$ , corresponding to  $(T_{10})_{\text{crit}} \sim 1.0$ , giving  $M_I \sim 1.35$ . If  $aB_0^2/q_* \approx 30$  ( $a \sim 0.4$  m,  $B_0 \sim 12.3$  T,  $q_* \sim 2$ ), then  $aB_0 \sim 4.9$ ,  $(T_{10})_{\text{crit}} \sim 1.1$ ,  $M_I \sim 2.0$ .

For a given scaling law, Eqs. (20) and (22) are used to generate ignition margin contours in  $(\langle n \rangle/n_{\text{mu}}, T)$  space. Results are summarized in Fig. 8 for several confinement scalings, where maximum attainable ignition margin within the plasma operating window are plotted against  $aB_0^2/q_*$ . Based on these results, devices with  $(aB_0^2/q_*) \sim 20 \pm 5$  appear ignitable with a margin  $M_I \sim 1.5 \pm 0.5$ .

#### 4.4 Auxiliary Power Requirements

Heating to ignition is discussed in detail in Ref. 20. The steady-state power balance equation [Eq. (20) with  $F \equiv \partial W/\partial t = 0$ ,  $P_{\text{aux}} \neq 0$ ] is used to produce auxiliary power contours for devices with given  $aB_0^2/q_*$  (see examples in Sect. 5 and discussions in Sect. 4.1). Figure 9 summarizes the results and shows the minimum auxiliary power required for ignition as determined by the maximum equilibrium power along the optimal density path (narrowest heating window) for several confinement models considered. Required auxiliary power for ignition decreases as  $aB_0^2/q_*$  increases. These are steady-state power requirements. Additional power is required for finite startup times, which is proportional to  $\Delta T \sim T_{\text{IGN}} - T_{\text{OH}}$  and inversely proportional to  $\Delta t$  heating (startup) time. For example, if  $\chi_e = \chi_{\text{NA}}$ ,  $\chi_i = 1 \times \chi_{\text{CH}}$ , and  $aB_0^2/q_* \sim 20$  (with  $a \sim 0.5$ ,  $B_0 \sim 9$  T,  $q_* \sim 2$ , and  $R_0/a \sim 3$ ), along the optimal density path ( $m_* \approx 0.8$ )  $T_{\text{OH}} \sim 3.5$  keV,  $T_{\text{IGN}} \sim 8.5$  keV [ $(\Delta T)_h \sim 5$  keV], and the plasma thermal energy content is about 16 MJ at  $T = T_{\text{IGN}}$ ,  $m = m_*$ . If this energy is added over a time interval of 3 s,  $\geq 5$  MW of excess power is required, essentially doubling the value [ $P_{\text{aux}}$  (equilibrium) = 6 MW] shown in Fig. 9. From Fig. 9 (and Figs. 4–6) we see that the possibility of ohmic ignition exists for devices with  $aB_0^2/q_* \sim 40 \pm 10$ .

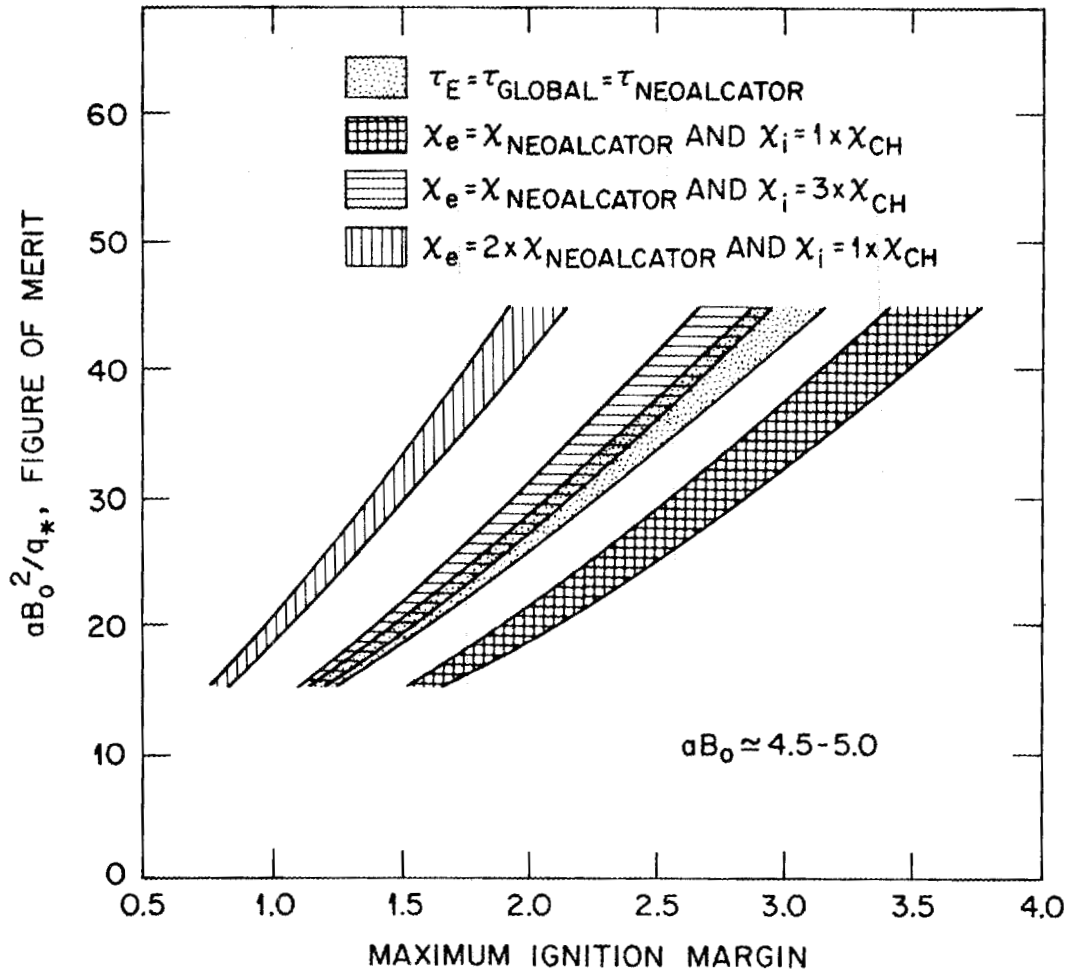


Fig. 8.  $aB_0^2/q_*$  vs maximum attainable ignition margin within the plasma operating window for several confinement scalings.

## 5. APPLICATIONS TO COMPACT TOKAMAK IGNITION EXPERIMENTS

Currently several candidate design options for a high-field, compact ignition experiment are being considered by the U.S. Tokamak Ignition Studies Design Teams.<sup>21</sup> These options include Ignitor-A,<sup>6</sup> PPPL-ISP,<sup>7</sup> and MIT-LITE.<sup>8</sup> Because these are design options and because detailed physics and engineering design studies are just beginning, we will not present their full parameter sets; rather we will treat them generically. From the physics point of view and in terms of our figure-of-merit parameter ( $aB_0^2/q_*$ ), the design options can be represented as two classes:

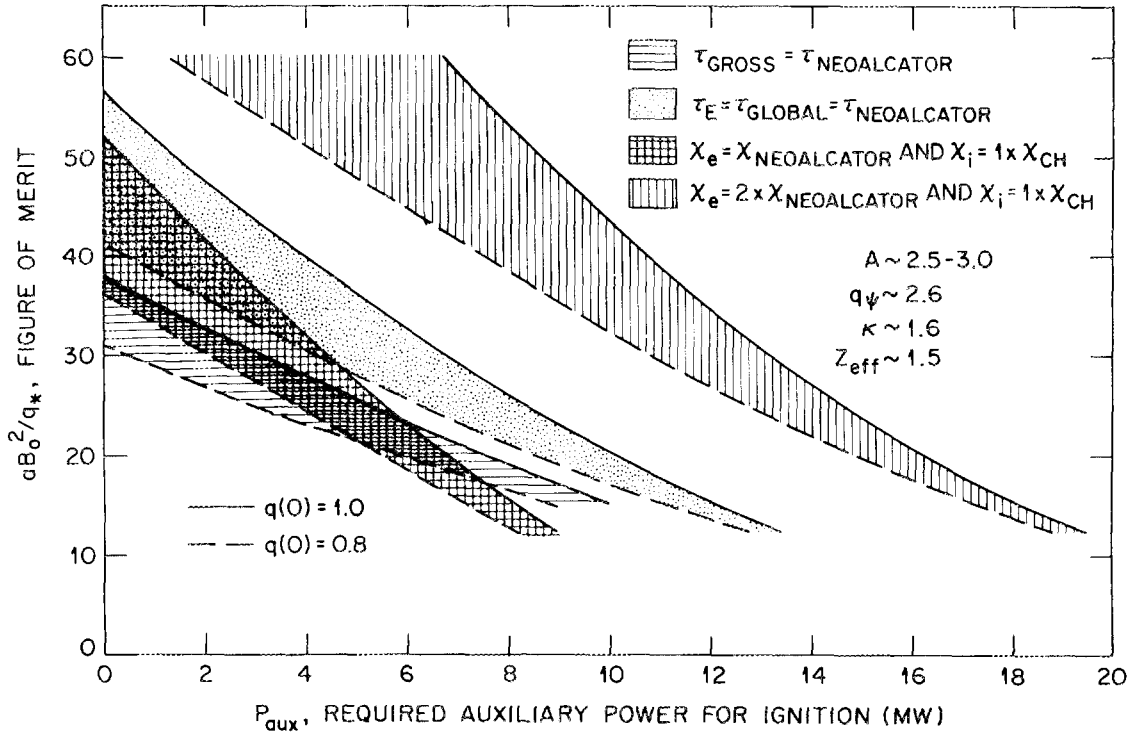


Fig. 9. Variation of steady-state auxiliary power required for ignition with  $aB_0^2/q_*$  for several confinement scalings.

1. Devices with  $aB_0^2/q_* \approx 20$  (PPPL-ISP<sup>7</sup> with  $a \sim 0.53$  m,  $R_0 \sim 1.6$  m,  $B_0 \sim 9$  T,  $I \sim 8$  MA,  $q_\psi \sim 2.6$ ,  $\kappa \sim 1.6$ ,  $\delta \sim 0.4$ ; MIT-LITE<sup>8</sup> with  $a \sim 0.55$  m,  $R_0 \sim 1.75$  m,  $B_0 \sim 8.5$  T,  $I \sim 7$  MA,  $q_\psi \sim 2.6$ ,  $\kappa \sim 1.6$ ,  $\delta \sim 0.3$ ).
2. Devices with  $aB_0^2/q_* \approx 32$  (Ignitor-A<sup>6</sup> with  $a \sim 0.39$  m,  $R_0 \sim 1$  m,  $B_0 \sim 12.6$  T,  $I \sim 10$  MA,  $q_\psi \sim 2.6$ ,  $\kappa \sim 1.67$ ,  $\delta \sim 0.25$ ).

For a typical range of aspect ratios ( $A \sim 2.5-3.0$ ) and  $q_* \sim 2.6$ , the range of device parameters corresponding to  $aB_0^2/q_* \sim 20-35$  is plotted in Fig. 10. The corresponding plasma current is  $I \sim 7-10$  MA [see Eq. (23)]. For most parameters, the range of interest is  $aB_0 \approx 4.5-5$ .

Standard parameters ( $\kappa = 1.6$ ,  $\delta \approx 0.2$ ,  $q_\psi \approx 2.6$ ,  $Z_{\text{eff}} \approx 1.5$ ,  $A \approx 3 \pm 0.5$ , etc.) assumed for the contour plots given in Sect. 4 are representative (within 10-15%) of ignition experiments; thus, any results given are directly applicable.

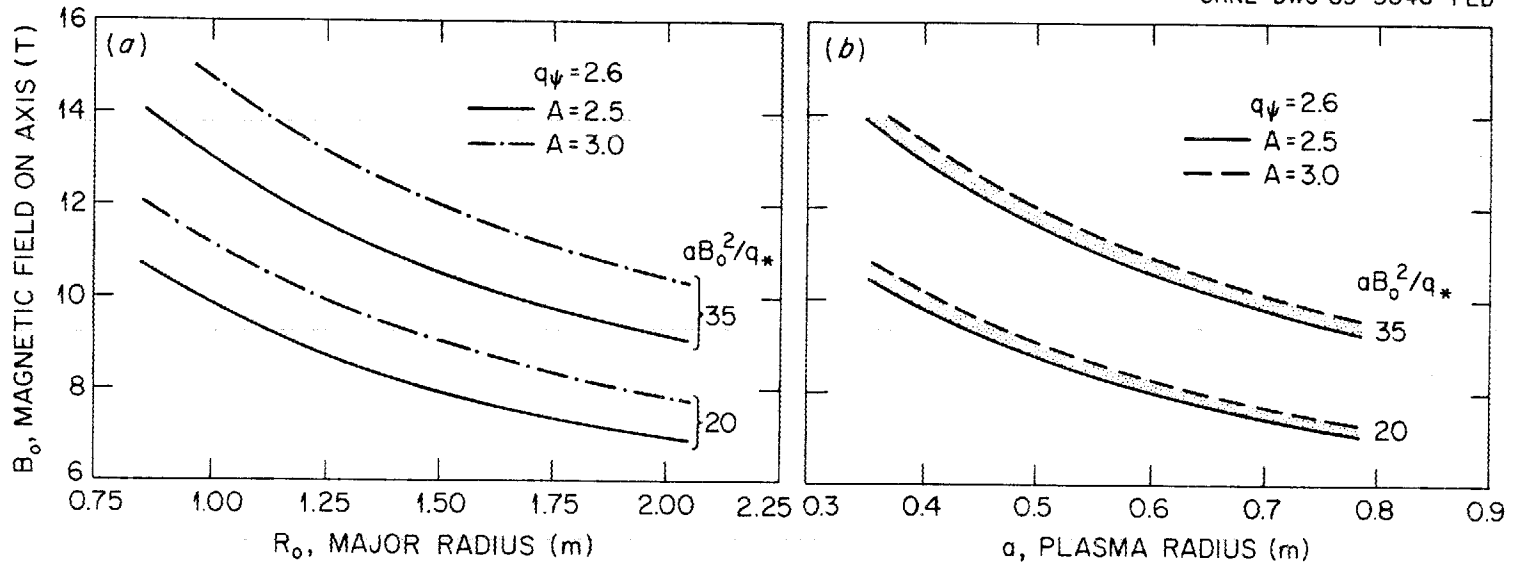


Fig. 10. Range-of-device parameters ( $B_0$ ,  $R_0$ ,  $a$ ) corresponding to  $aB_0^2/q_* = 20-35$  for typical aspect ratio range  $A \sim 2.5-3$  and  $q_\psi = 2.6$ .

### 5.1 Plasma Performance Contours for Devices with $aB_0^2/q_* \approx 20$

Steady-state auxiliary power contours [Eq. (20)] and critical beta contours [Eq. (30)] showing the ignition (and OH equilibrium), relative size of the heating and operating windows, and optimal density path are plotted in Fig. 11 for (1)  $\tau_E = \tau_{NA}$ , (2)  $\chi_c = \chi_{NA}$  and  $\chi_i = 1 \times \chi_{CH}$ , and (3)  $\chi_e = \chi_{NA}$  and  $\chi_i = 3 \times \chi_{CH}$ . In all cases  $q(0) = 0.8$  is assumed. Results are summarized in Table I.

### 5.2 Plasma Performance Contours for Devices with $(aB_0^2/q_*) \approx 32$

Steady-state auxiliary power contours, similar to Fig. 11, are given in Fig. 12. Results are summarized in Table II.

## 6. CONCLUSION

A simple analytic global model is developed for establishing ignition conditions and plasma parameter operating regimes over large regions of parameter space under various physics assumptions. This model has now been benchmarked against results from the 1/2-D WHIST transport code.<sup>9</sup> Analytic global calculations<sup>4</sup> reproduce many global features and trends of the 1/2-D transport calculations, especially those of POPCON, including ignition contours, auxiliary power requirements, optimal path to ignition, heating and operating windows, etc. Thus, this model is a useful complement to full 1/2-D code calculations because it allows a rapid assessment of a particular device; in addition, the ignition conditions and plasma parameter space may be formulated in terms of a small number of parameters such as  $aB_0^2/q_*$ ,  $\langle n \rangle/n_{mu}$ , and  $\langle T \rangle$  for analysis and/or assessment of classes of devices with equivalent performance.

The results from global calculations show that there exist regions in parameter space where a range of small ( $R_0 \sim 1-2$  m), high-field ( $B_0 \sim 8-13$  T) tokamaks appear ignitable. The results, however, depend on the transport properties (various forms of  $\chi_e$ ,  $\chi_i$ , and degradation at high power and  $\beta$ ), the neoclassical resistivity enhancement, the on-axis safety factor  $q(0)$  (which is associated with the sawtooth activity),  $Z_{eff}$ , etc. Based on the confinement scalings considered in this paper, the specific findings are as follows. (1) Ignition should be possible in devices with  $aB_0^2/q_* \sim 20 \mp 5$ ;  $P_{aux} \sim 10 \pm 5$  MW, provided  $\chi_e < (1.5 \mp 0.5)\chi_{NA}$  and  $\chi_i < (3 \mp 1)\chi_{CH}$ . (2) Prospects for ohmic ignition exist for devices with  $aB_0^2/q_* \sim 40 \mp 10$  under favorable assumptions for  $\chi_e$ ,  $\chi_i$ , and  $q(0)$ . Addition of a small amount of auxiliary heating ( $P_{aux} < P_{OH}$ ) could provide flexibility and increased margin. (3) Once ignited (by some means), devices with large  $aB_0^2/q_*$

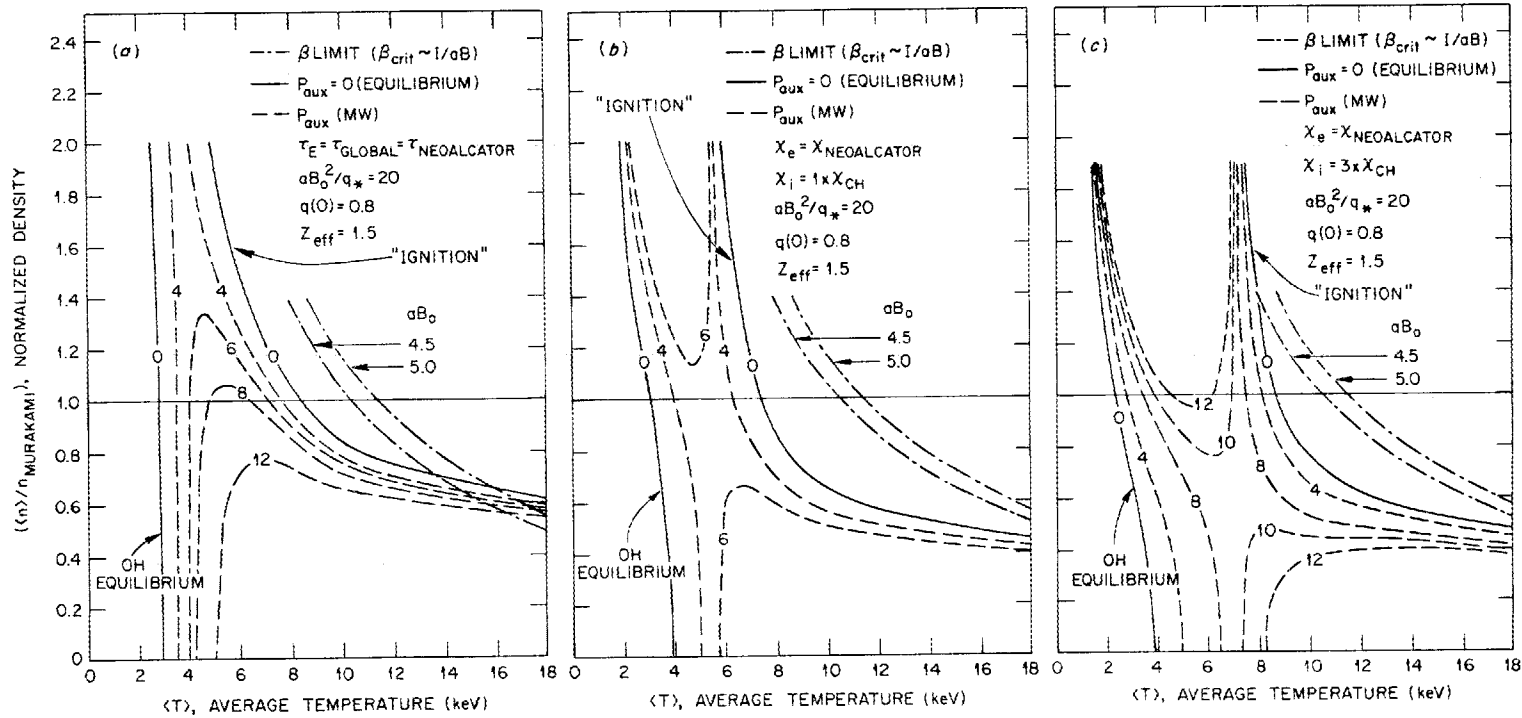


Fig. 11. Steady-state ( $\partial W/\partial t = 0$ ) auxiliary power contours and critical beta ( $\beta_{total} = \beta_{crit}$ ) contours for devices with  $aB_0^2/q_* \approx 20$  and  $q(0) \approx 0.8$ . **Confinement models:** (a)  $\tau_E = \tau_{neo-Alcator}$ , (b)  $\chi_e = \chi_{neo-Alcator}$  plus  $\chi_i = 1 \times \chi_{Chang-Hinton}$ , and (c)  $\chi_e = \chi_{neo-Alcator}$  plus  $\chi_i = 3 \times \chi_{Chang-Hinton}$ .

**Table I. Plasma performance for devices with  $aB_0^2/q_* \approx 20$** 

	$\tau_E = \tau_{NA}$	$\chi_e = \chi_{NA}$ $\chi_i = 1 \times \chi_{CH}$	$\chi_e = \chi_{NA}$ $\chi_i = 3 \times \chi_{CH}$
Optimal path <sup>a</sup> $\langle n \rangle / n_{mu}$	1.0	~0.85	~0.65
$P_{aux}$ (equilibrium) (MW)	~8.5	~5.5	~9.5
$(\Delta T)^b$ heating (keV)	~5.5	~4.5	~7-8
$(\Delta T)^b$ operating (keV)	~2.5	~5	~3-4
Maximum ignition margin	~1.5	~2	~1.4

<sup>a</sup>If optimal path is at  $m_* = \langle n \rangle / n_{mu} > 1$ ,  $m_* = 1$  is assumed.

<sup>b</sup>Measured at the optimal density path (results in Fig. 7 are measured at  $\langle n \rangle = n_{mu}$ ).

**Table II. Plasma performance for devices with  $aB_0^2/q_* \approx 32$** 

	$\tau_E = \tau_{NA}$	$\chi_e = \chi_{NA}$ $\chi_i = 1 \times \chi_{CH}$	$\chi_e = \chi_{NA}$ $\chi_i = 3 \times \chi_{CH}$
Optimal path <sup>a</sup> $\langle n \rangle / n_{mu}$	~1.0	~0.8	~0.65
$P_{aux}$ (equilibrium) (MW)	~3.5	~1.5	~5
$(\Delta T)^b$ heating (keV)	~3	~2	~4.5
$(\Delta T)^b$ operating (keV)	~5	~7.5	~7
Maximum ignition margin	~2.3	~2.8	~2.2

<sup>a</sup>If optimal path is at  $m_* = \langle n \rangle / n_{mu} > 1$ ,  $m_* = 1$  is assumed.

<sup>b</sup>Measured at the optimal density path (results in Fig. 7 are measured at  $\langle n \rangle = n_{mu}$ ).

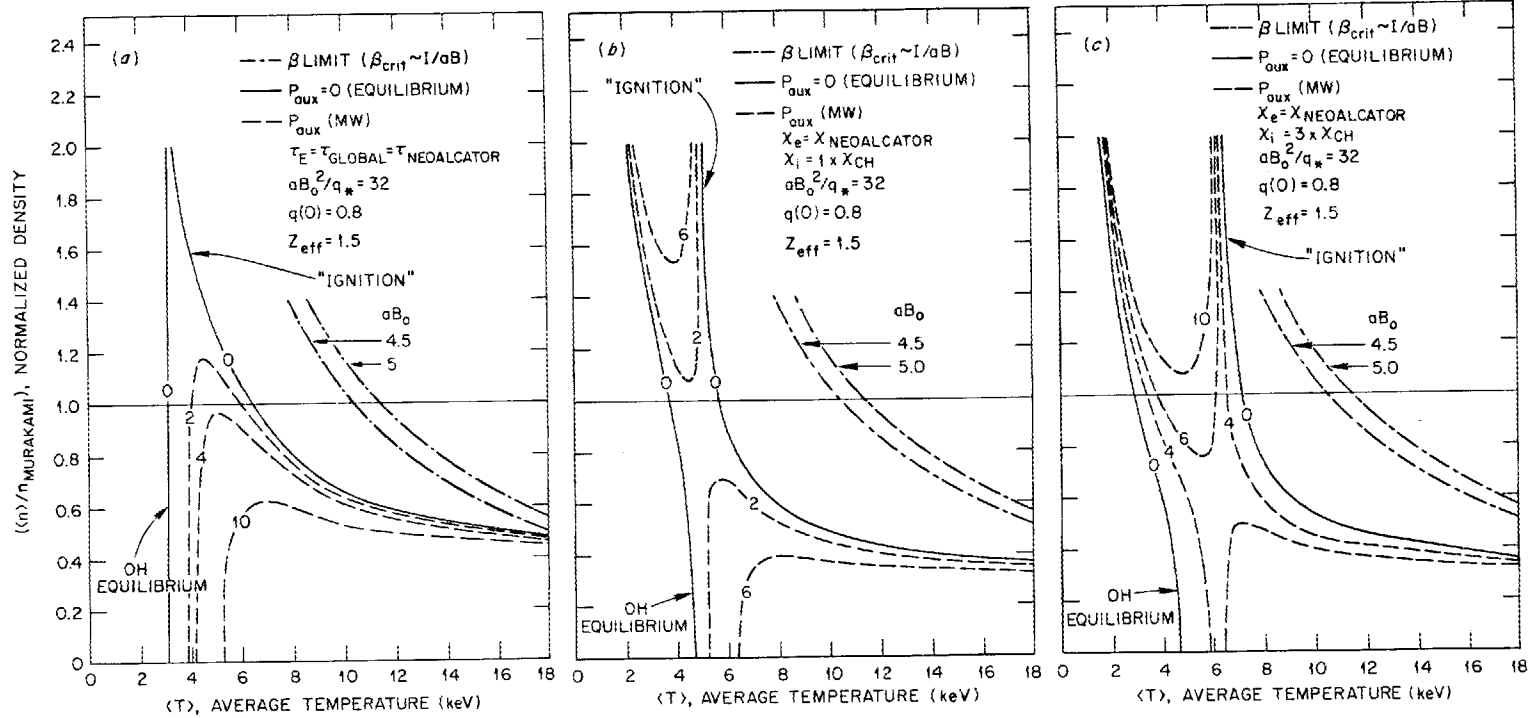


Fig. 12. Steady-state ( $\partial W/\partial t = 0$ ) auxiliary power contours and critical beta ( $\beta_{total} = \beta_{crit}$ ) contours for devices with  $aB_0^2/q_* \approx 32$  and  $q(0) \approx 0.8$ . Confinement models: (a)  $\tau_E = \tau_{neo-Alcator}$ , (b)  $X_e = X_{neo-Alcator}$  plus  $X_i = 1 \times X_{Chang-Hinton}$ , and (c)  $X_e = X_{neo-Alcator}$  plus  $X_i = 3 \times X_{Chang-Hinton}$ .

have favorable performance characteristics (large operating window, small heating window, large ignition margin, etc.), provided sufficient pulse length is available to benefit from these advantages.

## REFERENCES

1. J. Sheffield, "Options for an Ignited Tokamak," Oak Ridge National Laboratory Report ORNL/TM-8924 (1984).
2. N. A. Uckan, J. Sheffield, W. A. Houlberg, and E. C. Selcow, "Physics Scaling Studies for Tokamak Ignition Experiments" (to be published).
3. N. A. Uckan, J. Sheffield, and E. C. Selcow, A Simple Contour Analysis of Ignition Conditions and Plasma Operating Regimes in Tokamaks, presented at the 11th Symposium on Fusion Engineering, Austin, Nov. 18-22, 1985 (proceedings to be published).
4. N. A. Uckan, W. A. Houlberg, and J. Sheffield, Physics Evaluation of Compact Tokamak Ignition Experiments, presented at the 11th Symposium on Fusion Engineering, Austin, Nov. 18-22, 1985 (proceedings to be published).
5. M. Murakami et al., *Nucl. Fusion* 16:347 (1976).
6. B. Coppi, "An Advanced Burning Core Experiment," Massachusetts Institute of Technology R.L.E. Report PTP-84/17 (1984).
7. J. A. Schmidt et al., PPPL Ignition Studies Project, private communication, 1984-1985.
8. D. R. Cohn et al., MIT LITE Studies, private communication, 1984-1985.
9. W. A. Houlberg, private communication; see also W. A. Houlberg et al., *Nucl. Fusion* 22:935 (1982).
10. R. D. Hazeltine, F. L. Hinton, and M. N. Rosenbluth, *Phys. Fluids* 16:1645 (1973); B. Coppi and D. J. Sigmar, *Phys. Fluids* 16:1174 (1973).
11. B. Coppi, *Comments Plasma Phys. Controlled Fusion* 5:261 (1980).
12. Y-K. M. Peng, "Spherical Torus, Compact Fusion at Low Field," Oak Ridge National Lab. Report ORNL/FEDC-84/7 (1985).
13. F. Troyon et al., *Plasma Phys. Controlled Fusion* 26:209 (1984).
14. A. Sykes et al., paper B23 in: "Controlled Fusion and Plasma Physics (Proceedings of the 11th European Conference, Aachen, September 1983)," Part II, paper B23, 363 (1983).
15. C. S. Chang and F. L. Hinton, *Phys. Fluids* 25:1493 (1982).
16. R. J. Goldston, *Plasma Phys. Controlled Fusion* 26:87 (1984).
17. E. P. Gorbunov, S. V. Mirnov, and V. S. Strelkov, *Nucl. Fusion* 10:43 (1970).
18. S. M. Kaye and R. J. Goldston, *Nucl. Fusion* 25:65 (1985).
19. J. G. Cordey et al., p. 89 in: "Physics of Plasmas in Thermonuclear Regimes (Proceedings of the Varenna Workshop, 1979)," CONF-790866, U.S. Department of Energy (1981).
20. J. Sheffield, "Tokamak Startup—Problems and Scenarios Related to the Transient Phases of Ignited Tokamak Operations," presented at the Erice School on Tokamak Startup, Erice, Sicily, July 14-20, 1985; proceedings to be published.
21. U.S. Tokamak Ignition Studies Design Teams are located at Massachusetts Institute of Technology (IGNITOR-A, LITE), Oak Ridge National Laboratory, the Oak Ridge National Laboratory Fusion Engineering Design Center, Princeton Plasma Physics Laboratory, and TRW.



*INTERNAL DISTRIBUTION*

- |                     |  |
|---------------------|--|
| 1. L. A. Berry      | 17-21. J. Sheffield                                  |
| 2. T. G. Brown      | 22-26. N. A. Uckan                                   |
| 3. A. Dabiri        | 27. Y-K. M. Peng                                     |
| 4. R. A. Dory       | 28. E. C. Selcow                                     |
| 5. J. L. Dunlap     | 29. T. E. Shannon                                    |
| 6. C. A. Flanagan   | 30. T. Uckan   |
| 7. H. H. Haselton   | 31. K. L. Warren                                     |
| 8. J. T. Hogan      | 32-33. Laboratory Records Department                 |
| 9. W. A. Houlberg   | 34. Laboratory Records, ORNL-RC                      |
| 10. H. C. Howe      | 35. Document Reference Section                       |
| 11. E. A. Lazarus   | 36. Central Research Library                         |
| 12. G. H. Neilson   | 37. Fusion Energy Division Library                   |
| 13. J. B. Miller    | 38-39. Fusion Energy Division Publications<br>Office |
| 14. O. B. Morgan    | 40. ORNL Patent Office                               |
| 15. M. Murakami     |  |
| 16. M. J. Saltmarsh |  |

*EXTERNAL DISTRIBUTION*

41. M. A. Abdou, School of Engineering and Applied Science, 6288 Boelter Hall, University of California, Los Angeles, CA 90024
42. C. C. Baker, FPP/208, Argonne National Laboratory, 9700 South Cass Avenue, Argonne, IL 60439
43. C. Bolton, Office of Fusion Energy, Office of Energy Research, Germantown ER-55, U.S. Department of Energy, Washington, DC 20545
44. D. R. Cohn, The University of Texas at Austin, 26th and Speedway, Austin, TX 78712
45. R. W. Conn, Fusion Engineering and Physics Program, 6291 Boelter Hall, University of California, Los Angeles, CA 90024
46. B. Coppi, 77 Massachusetts Avenue, 26-217, Massachusetts Institute of Technology, Cambridge, MA 02139
47. R. C. Davidson, 77 Massachusetts Avenue, Massachusetts Institute of Technology, Cambridge, MA 02139
48. N. A. Davies, Office of Fusion Energy, Office of Energy Research, ER-55 Germantown, U.S. Department of Energy, Washington, DC 20545
49. S. O. Dean, Director, Fusion Energy Development, Science Applications, Inc., 2 Professional Drive, Suite 249, Gaithersburg, MD 20760
50. S. A. Eckstrand, Office of Fusion Energy, Office of Energy Research, ER-55 Germantown, U.S. Department of Energy, Washington, DC 20545
51. D. Ehst, Argonne National Laboratory, 9700 South Cass Ave., Argonne, IL 60439
52. G. A. Eliseev, I. V. Kurchatov Institute of Atomic Energy, P.O. Box 3402, 123182 Moscow, U.S.S.R.
53. A. J. Favale, Grumman Aerospace Corporation, MS-A0126, P.O. Box 31, Bethpage, NY 11714

54. H. K. Forsen, Bechtel Group, Inc., Research & Engineering, P.O. Box 3965, San Francisco, CA 94119
55. T. K. Fowler, Lawrence Livermore National Laboratory, P.O. Box 5511 (L-640), Livermore, CA 94550
56. H. P. Furth, Princeton Plasma Physics Laboratory, P.O. Box 451, Princeton, NJ 08544
57. J. R. Gilleland, GA Technologies, Inc., P.O. Box 85608, San Diego, CA 92138
58. V. A. Glukhikh, Scientific-Research Institute of Electro-Physical Apparatus, 188631 Leningrad, U.S.S.R.
59. R. J. Goldston, Princeton Plasma Physics Laboratory, P.O. Box 451, Princeton, NJ 08544
60. R. W. Gould, Department of Applied Physics, California Institute of Technology, Pasadena, CA 91125
61. C. D. Henning, Lawrence Livermore National Laboratory, P.O. Box 5511 (L-644), Livermore, CA 94550
62. T. R. James, Office of Fusion Energy, Office of Energy Research, ER-55 Germantown, U.S. Department of Energy, Washington, DC 20545
63. R. A. Krakowski, CTR-12, Mail Stop 641, Los Alamos National Laboratory, P.O. Box 1663, Los Alamos, NM 87545
64. G. L. Kulcinski, Department of Nuclear Engineering, University of Wisconsin, Engineering Research Building, Room 439, 1500 Johnson Drive, Madison, WI 53706
65. G. Logan, Lawrence Livermore National Laboratory, P.O. Box 5511 (L-644) Livermore, CA 94550
66. D. M. Meade, Princeton Plasma Physics Laboratory, P.O. Box 451, Princeton, NJ 08544
67. G. H. Miley, Nuclear Engineering Department, University of Illinois, Urbana, IL 61801
68. D. B. Montgomery, Massachusetts Institute of Technology, Plasma Fusion Center, 167 Albany Street, Cambridge, MA 02139
69. R. R. Parker, Massachusetts Institute of Technology, 170 Albany St., NW 16-288, Cambridge, MA
70. D. E. Post, Princeton Plasma Physics Laboratory, P.O. Box 451, Princeton, NJ 08544
71. D. Ross, The University of Texas at Austin, Fusion Research Center, Austin, TX 78712
72. P. H. Rutherford, Princeton Plasma Physics Laboratory, P.O. Box 451, Princeton, NJ 08544
73. D. D. Ryutov, Institute of Nuclear Physics, Siberian Branch of the Academy of Sciences of the U.S.S.R., Sovetskaya St. 5, 630090 Novosibirsk, U.S.S.R.
74. W. Sadowski, Office of Fusion Energy, Office of Energy Research, ER-55 Germantown, U.S. Department of Energy, Washington, DC 20545
75. J. A. Schmidt, Princeton Plasma Physics Laboratory, P.O. Box 451, Princeton, NJ 08544
76. W. M. Stacey, Jr., Georgia Institute of Technology, Fusion Research Center, Atlanta, GA 30332
77. R. D. Stambaugh, GA Technologies Inc., P.O. Box 85608, San Diego, CA 92138
78. D. Steiner, Rensselaer Polytechnic Institute, Department of Nuclear Engineering, Troy, NY 12181
79. P. M. Stone, Office of Fusion Energy, Office of Energy Research, ER-55 Germantown, U.S. Department of Energy, Washington, DC 20545
80. V. T. Tolok, Kharkov Physical-Technical Institute, Academical St. 1, 310108 Karkov, U.S.S.R.
81. R. Varma, Physical Research Laboratory, Navangpura, Ahmedabad, India
82. H. Weitzner, 251 Mercer St., New York University, New York, NY 10012
83. Bibliothek, Max-Planck-Institut für Plasmaphysik, D-8046 Garching bei München, Federal Republic of Germany
84. Bibliothek, Institut für Plasmaphysik, KFA, Postfach 1913, D-5170 Jülich, Federal Republic of Germany
85. Bibliothèque, Service du Confinement des Plasmas, CEA, B.P. No. 6, 92 Fontenay-aux-Roses (Seine), France

86. Documentation S.I.G.N., Department de la Physique du Plasma et de la Fusion Controlee, Association EURATOM-CEA, Centre d'Etudes Nucleaires, B.P. 85, Centre du Tri, 38041 Grenoble, Cedex, France
87. Library, Centre de Recherches en Physique des Plasmas, 21 Avenue des Bains, 1007 Lausanne, Switzerland
88. Library, Culham Laboratory, UKAEA, Abingdon, Oxfordshire, OX14 3DB, England
89. Library, FOM Instituut voor Plasma-Fysica, Rijnhuizen, Jutphaas, Netherlands
90. Library, Institute of Physics, Academia Sinica, Beijing, Peoples Republic of China
91. Library, Institute for Plasma Physics, Nagoya University, Nagoya 464, Japan
92. Library, International Centre for Theoretical Physics, Trieste, Italy
93. Library, JET Joint Undertaking, Abingdon, Oxfordshire, OX14 3DB, England
94. Library, Laboratorio Gas Ionizzati, Frascati, Italy
95. Plasma Research Laboratory, Australian National Laboratory, P.O. Box 4, Canberra, ACT 2000, Australia
96. Thermonuclear Library, Japan Atomic Energy Research Institute, Tokai, Naka, Ibaraki, Japan
97. Library, Plasma Physics Laboratory, Kyoto University, Gokasho Uji, Kyoto, Japan
98. Office of the Assistant Manager for Energy Research and Development, Department of Energy, Oak Ridge Operations, Oak Ridge, TN 37830
99. F. L. Ribe, College of Engineering, University of Washington, AERL Bldg. FL-10, Seattle, WA 98195
100. J. A. Maniscalco, TRW, 1 Space Park (R1/2128) Redondo Beach, CA 90278
101. D. Overskei, GA Technologies Inc., P.O. Box 85608, San Deigo, CA 92138
- 102-337. Given distribution as shown in TIC-4500, Magnetic Fusion Energy (Distribution Category UC-20 a,d,f,g: Plasma Systems, Fusion Systems, Experimental Plasma Physics, Theoretical Plasma Physics)